

## **MSc. Thesis VIBOT**

Jhimli Mitra

*Multispectral Image Processing Applied to Dermatology*

**Le2i, UMR CNRS 5158**, UFR Sciences and Techniques  
University of Burgundy

A Thesis Submitted for the Degree of  
MSc Erasmus Mundus in Vision and Robotics (VIBOT)

· 2009 ·

## **Abstract**

This thesis proposes two methods of quantification of the components underlying the human skin that are supposed to be responsible for the effective reflectance spectra of the skin over the visible wavelength. The first method is based on independent component analysis assuming that the epidermal melanin and the dermal haemoglobin absorbance spectra are independent of each other. The second method is based on the assumption that the absorbance spectra of oxy-haemoglobin and deoxy-haemoglobin contained in the blood vessels of the dermis of the skin are dependent components and thereby uses a simple matrix factorization technique with least squares estimation. Both methods extract the source spectra that correspond to the ideal absorbance spectra. The method based on independent component analysis provides feasible quantifications of each source component in the examined skin patch. The feasibility of the quantifications of the source components using the matrix factorization method has not been determined in this research.

*Freedom from the desire for an answer is essential to the understanding of a problem.*

...

J. Krishnamurti

# Contents

<b>Acknowledgments</b>	v
<b>1 Introduction</b>	1
1.1 The Human Skin . . . . .	2
1.1.1 Epidermis . . . . .	3
1.1.2 Dermis . . . . .	5
1.1.3 Subcutaneous Layer . . . . .	7
1.2 Optical Properties of Skin . . . . .	7
1.2.1 Cellular Absorption and Scattering . . . . .	7
1.2.2 Cutaneous Scattering . . . . .	8
1.3 Categories of Skin Diseases . . . . .	9
1.4 The ASCLEPIOS System . . . . .	11
<b>2 State of The Art of Source Separation</b>	13
2.1 Introduction . . . . .	13
2.2 Principal Component Analysis . . . . .	14
2.3 Independent Component Analysis . . . . .	15
2.3.1 Decorrelation is not independence . . . . .	16
2.3.2 Non-Gaussian distribution preferred . . . . .	17
2.4 Methods for Independent Component Analysis . . . . .	18

2.4.1	ICA by Maximizing Non-Gaussianity . . . . .	18
2.4.2	Maximum Likelihood Estimation for ICA . . . . .	20
2.4.3	ICA by Minimizing Mutual Information . . . . .	21
2.4.4	Tensorial Methods for ICA Estimation . . . . .	22
2.5	Previous Researches Related to Source Separation . . . . .	22
<b>3</b>	<b>Methodology</b>	<b>28</b>
3.1	Introduction . . . . .	28
3.1.1	Independent Component Analysis with Principal Component Analysis . .	29
3.1.2	Non-Negative Matrix Factorization (NNMF) . . . . .	33
<b>4</b>	<b>Results and Discussions</b>	<b>36</b>
4.1	Results for FastICA . . . . .	40
4.2	Results of NNMF . . . . .	41
<b>5</b>	<b>Conclusions and Future Works</b>	<b>46</b>
	<b>Bibliography</b>	<b>51</b>

# List of Figures

1.1	Benign and malignant skin atypia without significant visible differences. . . . .	1
1.2	Cross-sectional area of skin with different layers and components. . . . .	3
1.3	Layers of Epidermis of Human Skin, <i>Wikimedia Commons</i> . . . . .	4
1.4	Melanocytes and Keratinocytes in basal cell layer of the epidermis. ©1997, Procter and Gamble HairCare Research Centre . . . . .	5
1.5	The Dermis. ©2005, Alticor, Inc. . . . .	6
1.6	Logarithmic absorption coefficient values in the visible spectrum. . . . .	8
1.7	Schematic of optical pathways in skin. . . . .	9
1.8	A Schematic diagram of the ASCLEPIOS system . . . . .	11
2.1	Different types of kurtosis . . . . .	18
2.2	Contrast Functions . . . . .	20
4.1	Reconstructed reflectance of a pixel. . . . .	36
4.2	Ideal Reflectance Spectra for Oxy-haemoglobin, Deoxy-haemoglobin and Melanin	37
4.3	(i) Melanin and haemoglobin spectra obtained before fitting, (ii) Haemoglobin and melanin spectra after polynomial fit. . . . .	38
4.4	Reconstructed reflectance images. . . . .	39
4.5	Independent component analysis (i) Original skin patch, (ii) Supposed to be haemoglobin quantification, (iii) Supposed to be melanin quantification, (iv) haemoglobin and melanin spectra. . . . .	40

4.6	(i) Skin patch from café-au-lait spot, (ii) Obtained source spectra, (iii) Melanin quantification, (iv) Histogram of melanin quantification, (v) Haemoglobin quantification, (vi) Histogram of haemoglobin quantification . . . . .	42
4.7	(i) Skin patch from normal part, (ii) Obtained source spectra, (iii) Melanin quantification, (iv) Histogram of melanin quantification, (v) Haemoglobin quantification, (vi) Histogram of haemoglobin quantification . . . . .	43
4.8	(i) Skin patch comprising both café-au-lait and normal parts, (ii) Obtained source spectra, (iii) Melanin quantification, (iv) Histogram of melanin quantification, (v) Haemoglobin quantification, (vi) Histogram of haemoglobin quantification . . . .	44
4.9	Non-negative Matrix Factorization (i) Original skin patch, (ii) Supposed to be oxy-haemoglobin quantification, (iii) Supposed to be deoxy-haemoglobin quantification, (iv) oxy- and deoxy-haemoglobin spectra. . . . .	45

# Acknowledgments

The accomplishment of this research thesis would not have been possible without the supervision of my guide Dr. F. S. Marzani. Dr. Pierre Vabres of the University of Burgundy hospital provided huge support for the work by incorporating his expertise in the domain of dermatology and validating the feasibility of the results. I am thankful to the team M2D+ of the Le2i laboratory for providing me support on miscellaneous activities and a comfortable work environment. I would like to specially thank Mr. Romuald Jolivot (PhD student) and Mr. Thomas Decourselle (Scientific Engineer) for their continuous support and contribution in acquiring and processing of the skin data to produce the reflectance images and provide me a basic understanding of the system ASCLEPIOS. Finally, I would like to thank my husband Mr. Soumya Ghose, without whose support I would not have been able to complete the research work successfully.

# Chapter 1

## Introduction

Skin is the external covering of the human body and the largest part of the human *integumentary* system. Skin protects human from rain , wind, viruses, bacteria, friction, wound etc. and undergoes constant wear and tear. People do not tend to take much care of their skin unless some kind of irritation, rash or pigmentation is observed. In such situations people normally take help of dermatologists (skin specialists) for proper diagnosis and cure of the problem. Certain skin diseases are diagnosable just by observation with naked eye. However, there might be cases where skin biopsies are required that is a painfully invasive technique of diagnosis. As seen in figure 1.1 that, in cases of benign tumour called *nevus* and carcinogenic or malignant tumour called *melanoma*, there is no visible difference in the images, but, they provide significant histopathological differences i.e. differences in their cellular structures and chemical compositions when skin biopsies are done.



(i) A Typical Nevus ©2008,  
Logical Images Inc.



(ii) A Melanoma ©2007, Skin  
Cancer Awareness

Figure 1.1: Benign and malignant skin atypia without significant visible differences.

Researchers in the field of dermatology for the past two decades have tried to develop non-invasive techniques for diagnosis of skin diseases using cameras and exploiting the optical properties of skin [33, 34, 44]. The skin has different layers and each layer has different chemical components. Each of these chemical components have varied reflectance properties at different light spectrum. A device already in use is the spectro-photometer that measures the effective spectral reflectance for a skin patch over the visible spectrum. The M2D+ team of the Le2i laboratory has developed a device called **ASCLEPIOS** that takes into account the reflectance spectrum of the skin over a visible spectrum for each spatial pixel. The effective reflectance spectrum is the residue after the absorption and scattering of light by the underlying chemical components of the skin. Therefore, important analyses could be made regarding the quantification of the components in different skin layers for each skin *chromophore*. In this work, we assumed that the primary skin components (*chromophores*) that are responsible for absorption of light spectrum are *melanin* and *haemoglobin*. We proposed a method to separate the skin reflectance into the absorbance/reflectance spectra of melanin and haemoglobin respectively. Additionally estimations of the quantities of each of these components for each pixel are being made. Another method has been proposed to separate the components like *oxy-haemoglobin* and *deoxy-haemoglobin* present in the blood vessels underlying the skin. Therefore, two source separation algorithms have been proposed to separate the skin reflectance into its source components' reflectance. The first algorithm is based on the assumption that the absorbance/reflectance spectra of the underlying skin components are independent of each other, while the second algorithm assumes the dependency of the components' absorbance/reflectance spectra on one another.

In the remaining part of this chapter we would briefly describe the physiological structure of the human skin and the optical properties of skin, different categories of skin disease and a brief description of the system **ASCLEPIOS**.

## 1.1 The Human Skin

The skin is the outermost tissue of the human body. It is composed of multiple layers and protects the muscles, bones and internal organs. It is the largest part of the body contributing about 8% of body weight for an adult and with an area of approximately  $16,000\text{cm}^2$  [18]. Skin has a very complex structure and is made up of several components that contribute to the multilayered structure. Veins, capillaries, nerves, glands and different layers of tissues form a network under the skin. Skin is primarily composed of three layers, the *epidermis* the outermost layer, with the *dermis* underlying it and the *subcutaneous* layer or the hypodermis below the dermis. Figure 1.2 shows a cross-sectional area of the skin layers.

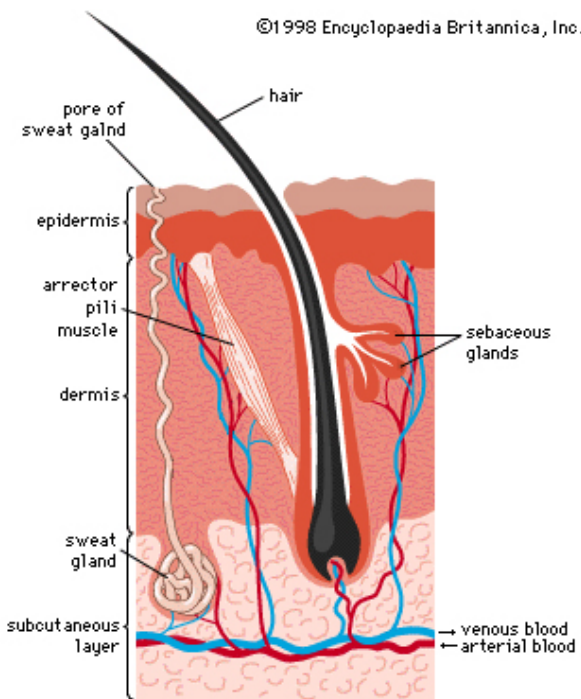


Figure 1.2: Cross-sectional area of skin with different layers and components.

### 1.1.1 Epidermis

The epidermis is the outermost layer of the skin, composed of terminally differentiated stratified *squamous epithelium* [25]. Its thickness is approximately 0.2mm on an average and varies with different parts of the body. It is the thinnest on the eyelids about 0.5mm and thickest on the palms and soles of feet of about 1.5mm. Epidermis is further divided into five more layers from the innermost to the outermost as *stratum basale* (*basal cell layer*), *stratum spinosum* (*prickle cell layer*), *stratum granulosum* (*granular cell layer*), *stratum lucidum* (*clear layer*) and *stratum corneum* (*horny cell layer*). Figure 1.3 shows the different layers of the epidermis.

**Stratum basale** is the deepest sublayer of the epidermis and is composed of a single layer of basal cells. This sublayer serves as a boundary to the dermis. Cells known as *keratinocytes* and *melanocytes* are found in this sublayer.

Keratinocytes are the major constituent of the epidermis and contribute about 95% and containing 8% of water of the epidermis. With aging these cells lose the ability to retain water and so the epidermis becomes thinner.

Melanocytes carry *melanin* which is one of the primary light absorbing pigments in the skin.

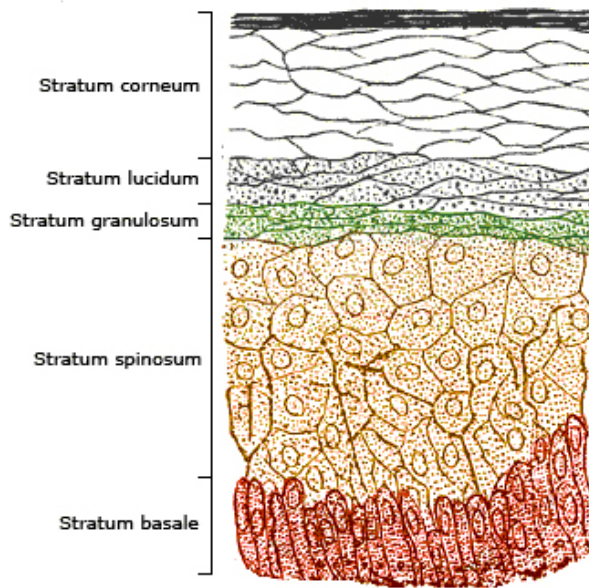


Figure 1.3: Layers of Epidermis of Human Skin, *Wikimedia Commons*

Around 1000 to 2000 melanocytes are found in  $1mm^2$  of skin. These cells are composed of special organelles called *melanosomes*. Through a process called *melanogenesis* the melanosomes produce melanin that is responsible for the pigmentation of the skin. Figure 1.4 shows melanocytes in the basal cell layer. Lighter-skinned people have lower levels of melanogenesis. Exposure to sun's UV-B radiation increases the level of melanogenesis. The difference in colour of skins is not due to the number of melanocytes present in the basal cell layer, but due to the quantity and relative amounts of *eumelanin* and *pheomelanin*, two different types of melanin whose production is under hormonal control. These two categories of melanin have different chemical structure. Eumelanin is a black to dark-brown insoluble material found in human black hair and the retina of the eye. Pheomelanin is a yellow to reddish-brown alkali-soluble material found in red hairs [30]. Sometimes in normal skin, eumelanin is present, therefore, in studies it is mostly referred to as melanin.

**Stratum Spinosum** is a sublayer of about 10 to 20 layers of cells above the basal cell layer. Its thickness is approximately  $50$  to  $150\mu m$ . Through the process of turn-over, the basal cells get flatter and form this layer. These cells have spines on the outer side of their membrane and hence are called prickle-cells. Langheran cells are present in this layer.

The Langheran cells are dendritic cells that are present in the epidermis and contain large granules called *Birbeck Granules*. These cells are normally present in the lymph node and other

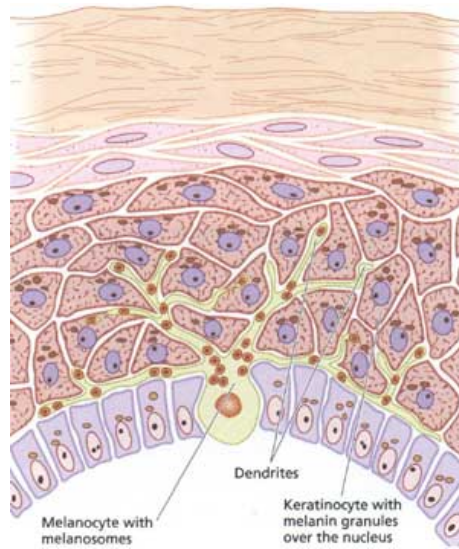


Figure 1.4: Melanocytes and Keratinocytes in basal cell layer of the epidermis. ©1997, Procter and Gamble HairCare Research Centre

organs including the stratum spinosum. On infection of a skin area, the Langerhans start the process of microbial antigens and become fully-functional antigen producing cells.

**Stratum Granulosum** has a thickness of about  $3\mu m$  and is composed of 5 to 10 layers of granular cells. In this layer the process of cornification or keratinization starts during which the cells are filled with keratin fibers and contain less moisture than the cells of the basal layer. The shape of the cells become much flatter during such process.

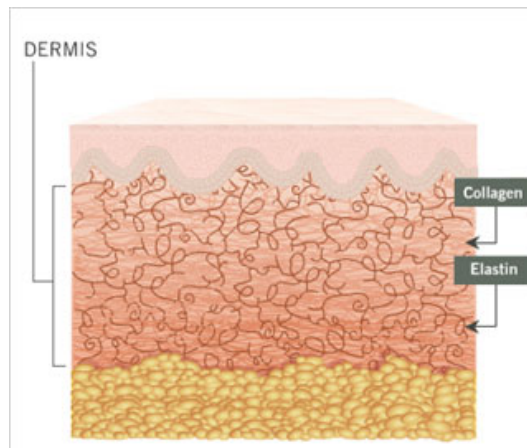
**Stratum Lucidum** sublayer contains cells that become flatter and more densely packed during turn-over. It is a highly refractive sublayer and can only be found in soles and palms.

**Stratum Corneum** is the outermost sublayer of the epidermis with a thickness of about 8 to  $15\mu m$ . It is composed of flat hexagonal cells that have dead organelles called corneocytes and are filled with keratin fibers. This sublayer prevents excess dehydration of the skin tissue and contributes to about 10 to 15% of mass of water in the epidermis.

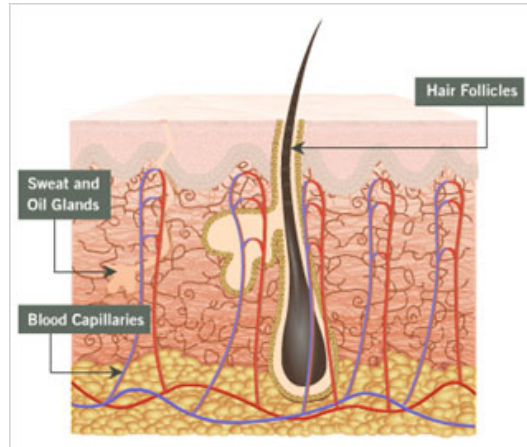
### 1.1.2 Dermis

It is the skin layer below the epidermis and is usually much thicker than the former. It is mainly composed of collagen and elastin fibers. A smaller sublayer of the dermis is the papillary layer that lies at the junction of the epidermis and dermis. The papillary layer contains a fine network of blood capillaries and nerve fibers and collagen tissue. Below the papillary layer is the reticular

layer that has less blood capillaries but densely packed with collagen and elastin fibers. Figure 1.5 shows the collagen and elastin fibers in the dermis and the network of blood vessels in it. The blood vessels carry blood. Red blood cells are called erythrocytes and contain another main light absorbing component of the skin called *haemoglobin* (Hb).



(i) Collagen and elastin fibers



(ii) Dermis networked with capillaries

Figure 1.5: The Dermis. ©2005, Alticor, Inc.

**Haemoglobin** is a light absorbing chromophore found in erythrocytes and constitutes 95% of the dry mass of an erythrocyte. It binds with oxygen easily and carries oxygen to every part of the body site through vessels and capillaries. Haemoglobin containing oxygen is called oxy-haemoglobin, else deoxy-haemoglobin or simply haemoglobin. Usually, in the veins, more

than 47% of the haemoglobin is oxy-haemoglobin. Oxy-haemoglobin is a brighter shade of red than deoxy-haemoglobin.

### 1.1.3 Subcutaneous Layer

The subcutaneous layer or hypodermis in histology, is the layer beneath the dermis. Subcutaneous layer is an elastic layer and includes a large amount of fat cells or adipose tissue that work as a shock absorber for blood vessels and nerve endings. The thickness of this layer is around 4 to 9mm on an average. The actual thickness however, differs from person to person and different body parts.

## 1.2 Optical Properties of Skin

Absorption of light in the skin over the visible spectrum is mainly caused by the chromophores, melanin and haemoglobin. While, scattering is caused by fibers, cells and organelles in different skin layers. Therefore, the absorption and scattering in the cellular level along with the scattering in the cutaneous level by fibers provide important information about the optical pathways in the skin.

### 1.2.1 Cellular Absorption and Scattering

Absorption of light in the skin over the visible spectrum is primarily due to the presence of melanin and haemoglobin. The absorption due to other cells and fibers is negligible. There has been a lot of research in measuring the absorption spectra of melanin and haemoglobin [1–3, 12, 20, 29, 33, 34, 44]. Figure 1.6 shows the absorption coefficient of haemoglobin, oxy-haemoglobin and melanin computed from the molar extinction coefficient data of haemoglobin and oxy-haemoglobin and the rule for computing the melanin absorption coefficient. Prahl [29] suggested that the data for the molar extinction coefficient ( $e$ ) in  $(cm^{-1}/(moles/liter))$  of haemoglobin and oxy-haemoglobin could be converted into the absorption coefficient ( $\mu_a$ ) in  $(cm^{-1})$  using the equation 1.1.

$$\mu_a = (2.303)e (x \text{ g/liter})/(64,500 \text{ g Hb/mole}) \quad (1.1)$$

$x$  is the molar concentration for the whole blood and is about 150 g Hb/liter. 64,500 g/mole is the gram molecular weight of haemoglobin (Hb).

Jacques [20] suggested a key-rule for computation of the melanin absorption coefficient in  $cm^{-1}$  depending on the wavelength ( $\lambda$ ) in nanometers(nm). The rule is given in equation 1.2.

$$\mu_a = 1.70 \times 10^{12} \times (\lambda)^{-3.48} \quad (1.2)$$

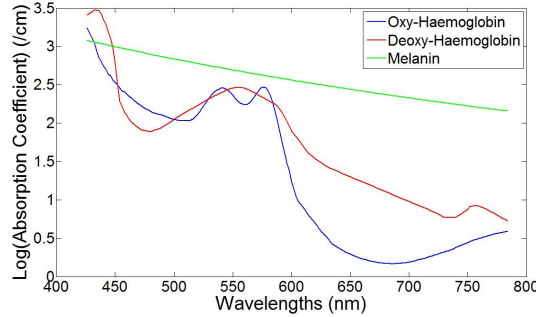


Figure 1.6: Logarithmic absorption coefficient values in the visible spectrum.

From figure 1.6 it is observed that the absorption by melanin decreases gradually with wavelength i.e. its colour is rich in red and poor in blue. The oxy- and deoxy-hemoglobin have local maxima in their absorption spectra in the short and middle wavelength ranges of the visible spectrum. The absorption spectrum of oxy-hemoglobin has a characteristic 'W' pattern around 550 nm indicating two maxima. While, the spectrum of deoxy-hemoglobin has a single peak at around 550 nm.

Scattering properties of the cellular level elements greatly depend on their refractive indices. The cells and fibers have higher refractive indices than the surrounding air medium and such a mismatch causes scattering. However, a melanin granule also has a very high refractive index, therefore, melanin is both a scatterer and absorber. When the size of a cellular level element is similar to the wavelength incident on it, the scattering properties of the element can be described by the *Mie Scattering*. In contrast, if the size of a cellular element is much smaller than the wavelength of light incident, then the scattering phenomenon could be described by the *Rayleigh Scattering* [6].

### 1.2.2 Cutaneous Scattering

Scattering in the skin layers is not the same as in the cellular level. The dermis is composed of collagen fibers, therefore, the scattering in this layer is the result of multiple scattering by the collagen fibers. However, the scattering in the epidermis is mainly due to the cellular elements.

Figure 1.7 [18] shows the schematic diagram of the optical pathway in different layers of the skin. Part of the incident light is reflected back on the surface of the skin. In the epidermis, light is being absorbed by melanin. In the dermal layer, light is being scattered multiple times

by the collagen fibers and absorbed by haemoglobin.

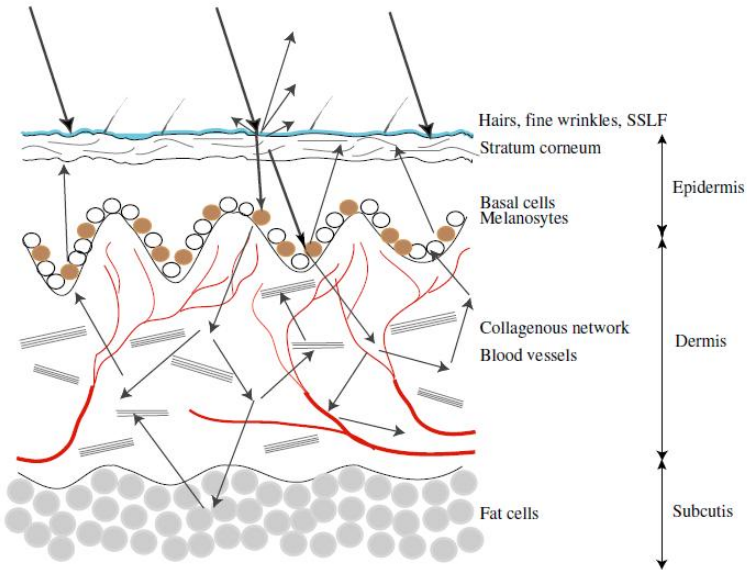


Figure 1.7: Schematic of optical pathways in skin.

### 1.3 Categories of Skin Diseases

Skin diseases can be broadly categorised into the following nine types. However, more than thousand conditions may exist as causes of skin diseases.

#### Rashes

A reddish inflamed skin or a group of spots is known as rash. These can be caused by allergy, irritation, infection of an existing disease and by structural defects e.g. blocked pores or malfunctioning of the sebaceous glands. Some common examples of rashes could be acne, dermatitis, eczema and psoriasis.

#### Viral Infections

When a virus penetrates the stratum corneum and infects the inner layers of the skin, a viral infection occurs. Examples of viral skin infections include herpes simplex, shingles (herpes zoster) and warts. Certain systemic viral infections, such as chicken pox or measles may also affect the skin.

## Bacterial Infections

Such infections can be caused by a variety of bacteria. The most common types of bacteria being the staphylococci and the streptococci. Bacteria may infect the topmost layers of skin, the follicles or the deeper layers of skin. However, these infections may spread throughout the body if not properly diagnosed and treated with antibiotics. The most common bacterial infections include impetigo, folliculitis, cellulitis and the Lyme disease.

## Fungal Infections

Fungi that are harmless are always present on surface of the skin. The infection occurs when these organisms enter the body. These infections usually affect the skin, hair and nails. Common fungal infections could be athletes foot, lock itch, and ringworm.

## Parasitic Infections

Exposure to parasites such as lice and scabies cause such type of infections.

## Pigmentation Disorders

Pigmentation in the skin is determined by the amount of melanin being produced in the area of skin. Loss of melanin is hypo-pigmentation and can be caused by an absence of melanocytes, malfunctioning of these cells, exposure to cold or chemicals, or some types of infection. Vitiligo is an example of hypo-pigmentation. Excess pigmentation or hyper-pigmentation may be caused by skin irritation, hormonal changes, aging, a metabolic disorder or any other problem. Age spots, freckles, café-au-lait spots and melasma are examples of hyperpigmentation.

## Tumors and Cancers

When skin cells begin to multiply faster than normal, tumours grow. Not every skin tumour is carcinogenic and are known as benign tumours that do not spread. Skin cancer is the most common of all the cancers, affecting 800,000 Americans each year. It is caused in 90 percent of cases by exposures to the UV radiation of sun. Skin cancers that are basal cell cancer are the most curable. Squamous cell cancers might grow and spread and malignant melanoma is the most deadly form of skin cancer.

## Trauma

Trauma can be described as an injury to the skin caused by a blow, cut or burn. Whenever the surface of the skin is broken, the body becomes more susceptible to infections and diseases.

## Other Conditions

Wrinkles, rosacea, spider veins, and varicose veins are among those conditions that cannot be clearly categorized. Wrinkles are caused by the breakdown of the collagen and the elastin fibers within the dermis of the skin. Rosacea is a long term disorder in which the facial skin becomes red and develops pimples, lesions and also sometimes enlargement of the nose. Spider veins and varicose veins become evident when blood vessels dilate and become visible through the surface of the skin.

## 1.4 The ASCLEPIOS System

ASCLEPIOS stands for Analysis of skin Characteristics by Light Emission and Processing by Imagery of Spectra. The system consists of a monochannel camera with a rotating wheel that holds the interference filters. It is driven by a dedicated software that controls the wheel and the image acquisition. The software manages a database and can perform signal and image processing on the acquired images. The system is exclusively dedicated to dermatological applications. Figure 1.8 shows a schematic diagram of the system.

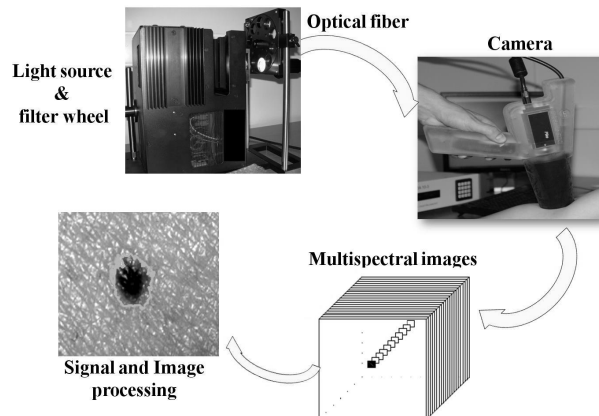


Figure 1.8: A Schematic diagram of the ASCLEPIOS system

The system is composed of a light source compartment with a Xenon light source that has a spectral property of being uniform in the range of  $380\text{ nm}$  and  $1000\text{ nm}$  wavelength. This compartment also consists of a holder for the rotating filter wheel. The hand-held device consists of the AVT PIKE CCD based monochrome camera (Allied Vision, Stradtrod, Germany). Optical fibres are used for the propagation of light from the light source to the hand-held

device for illumination of the skin area. A set of seven interference filters between the range of  $400\text{ nm}$  and  $800\text{ nm}$  is chosen to cover fully the spectral band. The interference filters are placed in the rotating wheel in front of the illumination source. The acquisition of images by the Pike camera is driven by the computer software that synchronises the rotating wheel of interference filters, the acquisition time and exposure. The camera acquires single band 16-bit images of resolution  $1280 \times 960$ . The seven single band images provide a stack of multispectral image. All the images are acquired in about  $2\text{ secs}$ .

## Chapter 2

# State of The Art of Source Separation

### 2.1 Introduction

Since, 1980's, researchers in the field of digital signal processing have been trying to solve a challenging problem of separating the source signals that combine to form a mixed signal. The classical problem in this domain is the cocktail-party problem where a number of people are talking simultaneously. It is possible for a human being to follow a discussion, because human brain can perform real-time processing of the mixed signal to separate into its respective components. However, the task of separating the sources of the signals is not simple for a machine.

A lot of work has been done in this direction based on Principal Component Analysis (PCA) and Independent Component Analysis (ICA). PCA is a classical statistical technique that aims to reduce redundancy from a mutivariate measurement by reducing the number of variables while maximally representing the original signal. PCA takes into account the correlation of the data elements and performs a linear projection of the data from the higher dimension to a lower dimension considering the eigen vectors and the eigen values obtained from the single-valued-decomposition of the covariance matrix of the data elements. However, this approach was extended to ICA to formulate a statistically stable model that is more than decorrelation and provides sources that are more relevant with a quantification of the sources in the mixed signal.

ICA [15, 17] assumes a model where the mixed signal is considered to be a linear mixture of sources with some noise that have been caused by the sensors used for the measurement. The

method basically tries to find components that are statistically independent and non-gaussian. If the mixture observed is considered as  $x_j(t)$  where,  $t = 1, \dots, T$  represents the number of observed mixtures and  $j = 1, \dots, m$  is the number of variables used to represent a mixture. The problem can be formulated in two ways.

Firstly, the mixtures could be represented as a linear combination of the independent components. Therefore,  $x_j(t)$  are the weighted sums of source signals  $s_i(t)$ ,  $i = 1, \dots, n$ .

$$x_j(t) = \sum_i a_{ij} s_i(t) \quad (2.1)$$

$a_{ij}$  are the mixing coefficients that determine the amount of each independent source in the mixture. However, the mixing coefficients  $a_{ij}$  and the sources  $s_i$  underlying the mixtures are assumed to be unknown. Therefore, the problem could be formulated as a *blind source separation* (BSS) problem where very little can be assumed about the underlying original sources. It can be assumed that the coefficients  $a_{ij}$  are quite different and can form an invertible matrix  $\mathbf{W}$ . The matrix  $\mathbf{W}$  consists of the coefficients  $w_{ij}$  and separate sources  $s_i$  as

$$s_i(t) = \sum_j w_{ij} x_j(t) \quad (2.2)$$

Therefore, the problem is to find the coefficients  $w_{ij}$  of the matrix  $\mathbf{W}$  and a surprisingly simple solution is to assume statistical *independence* and the *non-Gaussianity* of the source signals.

## 2.2 Principal Component Analysis

Principal Component Analysis (PCA) aims to find from a multivariate measurement, a smaller set of variables with reduced redundancy that would give a representation as good as possible. The redundancy is measured by correlations between the data elements [15].

Let us assume a random vector  $\mathbf{x}$  with  $n$  elements,  $x(1), x(2), \dots, x(T)$  whose principal components are to be found. Neither any assumption about the density nor about the model of the random vector is required in PCA as long as the first-order statistics (mean) and second-order statistics (variance) are known. In PCA, the vector is first centered by subtracting its mean and thus making  $E\{\mathbf{x}\} = 0$  as

$$\mathbf{x} \leftarrow \mathbf{x} - E\{\mathbf{x}\} \quad (2.3)$$

Then a linear transformation of  $\mathbf{x}$  into  $\mathbf{y}$  of  $m$  elements, where,  $m < n$  is done to reduce the redundancy in the correlations. This transformation is done by finding a rotated orthogonal coordinate system such that the elements of  $\mathbf{x}$  in the new coordinate system are uncorrelated

and also the variances of the projections of  $\mathbf{x}$  on the new axes are maximized so that the first axis has the maximal variance and the axis with next maximum variance is the one orthogonal to the previous and so on. The orthogonal transformation is achieved using linear algebra methods of matrix factorization into eigen vectors and eigen values. The  $n \times n$  covariance of the centered data  $\mathbf{x}$  is denoted by

$$C_{\mathbf{x}} = E \{ \mathbf{x} \mathbf{x}^T \} \quad (2.4)$$

The Eigen factorization of the matrix  $C_{\mathbf{x}}$  yields an eigen matrix whose columns are unit length vectors called eigen vectors  $\mathbf{e}_1, \mathbf{e}_2, \dots, \mathbf{e}_n$  and a diagonal matrix whose diagonal non-zero elements are called the eigen values corresponding to the eigen-vectors such that the values are  $d_1 \geq d_2 \geq d_3 \geq \dots \geq d_n$ . The solution maximizing the variance is the eigen-vector  $\mathbf{e}_1$  and the first principal component is given by

$$y_1 = \mathbf{e}_1^T \mathbf{x} \quad (2.5)$$

## 2.3 Independent Component Analysis

Independent Component Analysis (ICA) means separation of components that are independent to each other from mixtures of signals. Instead of writing the sources and mixtures in the form of summation as in the previous equations, it is convenient to write them in a vector-matrix form of equation 2.6.  $\mathbf{x}$  is a random vector with mixtures  $x_1, \dots, x_n$  and  $\mathbf{s}$  is a random vector of components  $s_1, \dots, s_n$ .  $\mathbf{A}$  is a matrix of mixing coefficients  $a_{ij}$ . The vectors are column vectors.

$$\mathbf{x} = \mathbf{As} \quad (2.6)$$

The principal assumptions in the model of ICA is that the sources are statistically *independent, non-Gaussian* [17] and number of mixtures is equal to the number of source components and therefore, the mixing matrix  $\mathbf{A}$  is a square matrix and is easy to estimate. However, there could be cases in which the number of sources are less than the number of mixtures that will be treated separately in subsequent chapters. Another important aspect to be considered at this point is that decorrelation is only half the ICA model and that is why only PCA or factor analysis does not produce components that are independent, but are decorrelated. The decorrelation of the observed signals achieved by PCA is often known as *whitening* or *sphering*.

### 2.3.1 Decorrelation is not independence

Let us assume two zero-mean random variables as  $y_1$  and  $y_2$ . Thus, the covariance is equal to correlation  $\text{corr}(y_1, y_2) = E\{y_1 y_2\}$ , where,  $E\{\cdot\}$  is the expectation. Uncorrelatedness means zero correlation. Therefore, if the random variables are independent, they are uncorrelated and for any function  $h_1$  and  $h_2$ ,

$$E\{h_1(y_1)h_2(y_2)\} = E\{h_1(y_1)\} E\{h_2(y_2)\} \quad (2.7)$$

However, uncorrelatedness does not always imply *independence*. If  $(y_1, y_2)$  are a pair of discrete values that follow a distribution such that each pair has a probability of 1/4 and has any of the following values  $(0, 1), (0, -1), (1, 0), (-1, 0)$ . Then  $E\{y_1 y_2\} = E\{y_1\} E\{y_2\}$  holds, i.e. the variables are uncorrelated, but,

$$E\{y_1^2 y_2^2\} = 0 \neq \frac{1}{4} = E\{y_1^2\} E\{y_2^2\} \quad (2.8)$$

Therefore, in this case even if the variables are uncorrelated, the condition of independence in equation 2.7 does not hold and so decorrelation is a *weaker form* of *independence*. A stronger form of independence could be *whitening*, where not only the random variables are decorrelated but their variance is also unity, i.e. their covariance matrix is equals to identity.

$$E\{yy^T\} = I \quad (2.9)$$

Whitened data is a linearly transformed observed data after multiplying it with some matrix  $\mathbf{V}$ .

$$\mathbf{z} = \mathbf{V}\mathbf{x} \quad (2.10)$$

$\mathbf{z}$  is the whitened data. The detailed method about this linear transformation has been discussed in chapter 3. From equation 2.6 and equation 2.10 we have

$$\mathbf{z} = \mathbf{V}\mathbf{A}\mathbf{s} = \tilde{\mathbf{A}}\mathbf{s} \quad (2.11)$$

The whitening procedure transforms the mixing matrix into a new one  $\tilde{\mathbf{A}}$ . However, this whitening is not enough to get the independent components. If an orthogonal transformation is given to the whitened data  $\mathbf{z}$ ,

$$\mathbf{y} = \mathbf{U}\mathbf{z} \quad (2.12)$$

Due to the orthogonality of  $\mathbf{U}$  and the covariance of the whitened data equals to identity,

$$E \{ \mathbf{y} \mathbf{y}^T \} = E \{ \mathbf{U} \mathbf{z} \mathbf{z}^T \mathbf{U}^T \} = \mathbf{U} \mathbf{I} \mathbf{U}^T = \mathbf{I} \quad (2.13)$$

Therefore,  $\mathbf{y}$  is also white and it is not possible to ascertain whether the independent components are given by  $\mathbf{z}$  or  $\mathbf{y}$ .  $\mathbf{y}$  can be any orthogonal transformation of  $\mathbf{z}$ . Nevertheless, *whitening* is an important preprocessing step of independent component analysis as it transforms the mixing matrix into an orthogonal matrix and therefore, the search of the mixing matrix remains restricted in the space of orthogonal matrices.

### 2.3.2 Non-Gaussian distribution preferred

The central limit theorem states that the linear combination of two random distributions that are Gaussian is necessarily also Gaussian. Therefore, the joint probability density function (pdf) of the two independent components  $s_1$  and  $s_2$  that are Gaussian can be represented as

$$p_s(s_1, s_2) = \frac{1}{2\pi} \exp\left(-\frac{s_1^2 + s_2^2}{2}\right) = \frac{1}{2\pi} \exp\left(-\frac{\|s\|^2}{2}\right) \quad (2.14)$$

From the fact that  $\mathbf{A}$  is orthogonal because the data is whitened,  $\mathbf{A}^{-1} = \mathbf{A}^T$ . Since, the independent components (ICs) are multivariate Gaussians, the mixtures are also multivariate Gaussians and are related by equation 2.6. Therefore, to get the pdf of the mixtures  $x_1$  and  $x_2$  from the pdf of the ICs, we have

$$p_x(x_1, x_2) = \frac{1}{|\det \mathbf{A}|} p_s(\mathbf{A}^{-1} \mathbf{x}) \quad (2.15)$$

Combining equation 2.14 and equation 2.15 we get the pdf of the mixtures as

$$p_x(x_1, x_2) = \frac{1}{2\pi} \exp\left(-\frac{\|\mathbf{A}^T \mathbf{x}\|^2}{2}\right) \frac{1}{|\det \mathbf{A}|} \quad (2.16)$$

$$p_x(x_1, x_2) = \frac{1}{2\pi} \exp\left(-\frac{\|\mathbf{x}\|^2}{2}\right) \quad (2.17)$$

Since,  $\mathbf{A}$  is orthogonal,  $|\det \mathbf{A}| = 1$  and  $\|\mathbf{A}^T \mathbf{x}\|^2 = \|\mathbf{x}\|^2$ . Therefore, from equation 2.17 we observe, that the orthogonal mixing matrix does not appear in the pdf and the pdf of the original components and the mixtures are identical. Hence, separation of Gaussian random variables into independent components is not achievable using ICA and the mixing matrix cannot be estimated using Gaussian variables. For Gaussian variables, independence is achieved only upto whitening.

## 2.4 Methods for Independent Component Analysis

### 2.4.1 ICA by Maximizing Non-Gaussianity

In the last section it has been observed that non-Gaussianity is of importance in ICA estimation. Therefore, maximizing non-Gaussianity could be a key to the process of ICA. Non-Gaussianity of a signal can be measured statistically using *kurtosis* and in information-theoretic concept by a term called *negentropy*.

#### Kurtosis as a measure of non-Gaussianity

Kurtosis of a random variable is a fourth-order cumulant and is a classical measure of non-Gaussianity. In ICA estimation, the idea is to maximize the non-Gaussianity of the independent components by maximizing the absolute value of their kurtosis [16]. Kurtosis means 'peakedness' of a random variable. A random variable  $y$  could be leptokurtic (super Gaussian), platykurtic (sub Gaussian) or mesokurtic (Gaussian). The kurtosis values for super-Gaussian and sub-Gaussian distributions are *positive* and *negative* respectively. While, for Gaussian distributions kurtosis is zero. Kurtosis of a random variable may be defined as

$$\text{kurt}(y) = E \{y^4\} - 3(E \{y^2\})^2 \quad (2.18)$$

Figure 2.1 shows the different distributions of positive, negative and zero kurtosis.

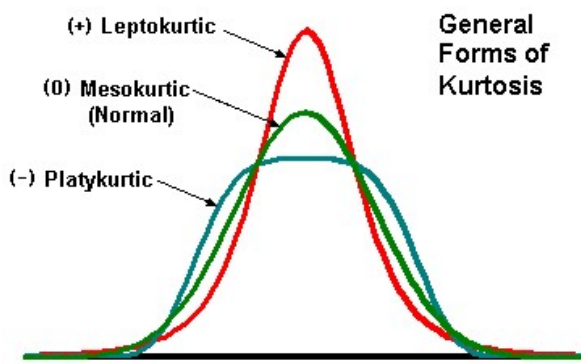


Figure 2.1: Different types of kurtosis

Since non-Gaussianity is measured by positive or negative kurtosis, the absolute value of kurtosis is maximized in ICA estimation.

### Negentropy as a measure of non-Gaussianity

Hyvärinen [14] combined the *differential entropy* concept of Comon [11] for maximizing non-Gaussianity of random variables in ICA estimation. Differential entropy or simply entropy gives the amount of information in the observed random variable. The more unstructured and random a variable is, the more is the entropy related to it. Differential entropy is given by equation 2.19, where,  $f(\cdot)$  is the pdf of the random variable.

$$H(y) = - \int f(y) \log f(y) dy \quad (2.19)$$

A Gaussian random variable has the largest differential entropy. Therefore, as a measure of non-Gaussianity i.e. zero for a Gaussian variable, a normalized version of differential entropy known as *negentropy* could be used. Negentropy of a random variable is given in equation 2.20.

$$J(y) = H(gauss) - H(y) \quad (2.20)$$

The larger the negentropy, the more is the non-Gaussianity. Negentropy is always positive therefore for ICA estimation the primary objective would be to maximize the negentropy of the independent components. However, computation of negentropy is complicated and expensive. Hence, an approximation of negentropy was suggested by Hyvärinen [14] through a set of contrast functions.

A contrast function is a non-linear function that is invariant to permutation and scaling matrices and always reaches an optimum in correspondence to mutual independence of the sources. A typical choice of the contrast function is the kurtosis that is maximized in case of super-gaussian distribution and minimized in case of sub-gaussian distribution of the sources.

The approximation of negentropy is given as in equation 2.21.

$$J(y) \approx [E\{G(y)\} - E\{G(\nu)\}]^2 \quad (2.21)$$

A contrast function should be a non-linear function that does not grow too fast. Therefore, the functions in equation 2.22 and equation 2.23 are good choices of non-linearity.

$$G(y) = \frac{1}{a_1} \log \cosh a_1 y \quad (2.22)$$

$$G(y) = -\exp(-y^2/2) \quad (2.23)$$

$1 \leq a_1 \leq 2$  gives good choices of non-linearity. Figure 2.2 shows the graphical representations of the contrast functions. The solid line is the function in equation 2.22 and the dashed line is the function in equation 2.23. Therefore, such approximations of negentropy are easy to

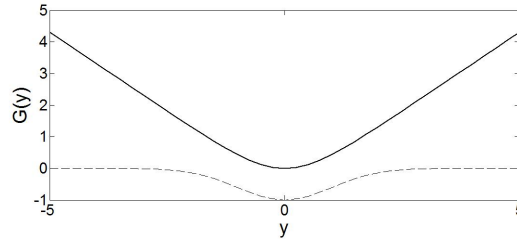


Figure 2.2: Contrast Functions

compute and combines the functionality of both measures of non-Gaussianity as kurtosis and negentropy.

The optimization algorithm for both the methods of maximizing non-Gaussianity is achieved by either gradient or fixed-point methods. FastICA is one such fixed-point iteration optimization algortihm that will be discussed in chapter 3.

#### 2.4.2 Maximum Likelihood Estimation for ICA

A very popular approach of ICA estimation is Maximum Likelihood Estimation (MLE). An interpretation of MLE could be that only those estimates of parameters are considered that give the highest probability density of the observations. MLE in ICA estimation can be applied in the following manner.

The pdf of a linear transformation  $\mathbf{x} = \mathbf{As}$  can be obtained from equation 2.15 as follows:

$$p_x(\mathbf{x}) = |\det \mathbf{B}| p_s(s) = |\det \mathbf{B}| \prod_i p_i(\mathbf{s}_i) \quad (2.24)$$

$p_x$  is the density of the mixture vector,  $\mathbf{B} = \mathbf{A}^{-1}$  and  $p_i$  are the densities of the independent source components. If  $\mathbf{B} = [b_1, \dots, b_n]^T$ , then equation 2.24 combined with equation 2.15 can be written as

$$p_x(\mathbf{x}) = |\det \mathbf{B}| \prod_i p_i(\mathbf{b}_i^T \mathbf{x}) \quad (2.25)$$

If  $T$  observations of  $\mathbf{x}$  are assumed as  $x(1), \dots, x(T)$ , then the likelihood ( $L$ ) as a function of  $\mathbf{B}$  can be expressed as

$$L(\mathbf{B}) = \prod_{t=1}^T \prod_{i=1}^n p_i(\mathbf{b}_i^T x(t)) |\det \mathbf{B}| \quad (2.26)$$

Likelihood is often replaced by its logarithm for algebraic simplicity and is represented as

$$\log L(\mathbf{B}) = \sum_{t=1}^T \sum_{i=1}^n \log p_i(\mathbf{b}_i^T \mathbf{x}(t)) + T \log |\det \mathbf{B}| \quad (2.27)$$

Therefore,

$$\frac{1}{T} \log L(\mathbf{B}) = E \left\{ \sum_{i=1}^n \log p_i(\mathbf{b}_i^T \mathbf{x}) \right\} + \log |\det \mathbf{B}| \quad (2.28)$$

The expectation here is not a theoretical one and is only the sample average of the observations. The problem in likelihood estimation lies upto the estimation of the inverse of the mixing matrix  $\mathbf{B}$  until this point. However, parameters of the densities of the independent components also need to be estimated in the MLE. The densities of the independent components are unknown in most cases and hence a non-parametric estimation is required. Non-parametric estimation often is time consuming as a large number of finite parameters are to be estimated. Sometimes a prior knowledge about the densities of the independent components facilitate by assuming a density distribution with a smaller number of parameters to be estimated. Though this assumption might not be correct in all cases and often lead to wrong estimation. Also, it is not always possible to categorize the distribution of the independent components into specific density families.

The optimization lies in the numerical maximization of the likelihood and is often achieved by the Bell-Sejnowski algorithm [15, ch.9], natural gradient and Fast Fixed-Point (FastICA) methods.

### 2.4.3 ICA by Minimizing Mutual Information

This method of ICA estimation is an extension of the concept of negentropy as discussed previously. Mutual information is a measure of dependence among the random scalar values of  $y_i$ ,  $i = 1, 2, \dots, n$ . Using such a measure, ICA could be defined as a linear decomposition that minimizes such dependence measure. Mutual information in terms of negentropy of equation 2.20 could be derived [15, ch.10] [14] as

$$I(y_1, y_2, \dots, y_n) = J(y) - \sum_i J(y_i) \quad (2.29)$$

Minimizing the mutual information basically means maximising the negentropy  $J(y_i)$  i.e. the sum of non-Gaussianities of the estimates of the independent components. The optimization can be achieved using the gradient methods or FastICA.

#### 2.4.4 Tensorial Methods for ICA Estimation

The fourth-order cumulant of mixtures give all the fourth-order information inherent in the data. A tensor can be defined using the fourth-order cumulant i.e. the generalization of a covariance matrix. Then eigen-value decomposition (EVD) can be applied on this tensor matrix and the eigen vectors more or less directly give the mixing matrix of the whitened data. The most general method for EVD is the power method. However certain variations like the Joint Approximate Diagonalization of Eigen matrices (JADE) algorithm [8] [9] can be used if the dimensionality of the data is low. If the independent components have very distinct kurtosis, then the Fourth-Order Blind Identification (FOBI) algorithm [10] is another approach of tensor factorization. These algorithms however, are statistically inferior than the likelihood estimation but provide interesting results in cases where the data dimensionality is low.

Belouchrani et al. [4] developed a technique with a possibility of separating Gaussian sources and that are temporally correlated using only the joint diagonalization of second-order cumulants i.e. covariance matrices and called it the Second-Order Blind Identification (SOBI) algorithm.

### 2.5 Previous Researches Related to Source Separation

Independent Component Analysis proved to be a powerful estimation tool in various fields of research, from analysis of satellite images to medical images.

Farah et al. [13] proposed decomposition of a pixel of satellite images into the number of constituent sources using the FASTICA2D, JADE2D and SOBI2D (Second-order blind identification 2D) algorithms adapted to operate in 2D context. Then based on the maximum entropy of the sources a fusion algorithm was used based on Maximum Likelihood Classification to classify each pixel into a specific class as humid, urban, sebkht, parcel and cultivated zones. The fusion algorithm was carried out using the source images obtained from source separation methods and the training signatures for the different zones to classify. Each source image was used to determine the percentage of pixels belonging to a particular zone using the source image with maximum entropy. The maximum rate of classification obtained was 98%.

Robila [31] modified the ICA method of blind source separation by developing a distributed system for faster computation and convergence. The method was applied to hyperspectral satellite images from AVIRIS and HYDICE. The ICA optimization was based on the minimisation of mutual information after reducing the data set into a number of components that mostly represent the entire dataset. This was achieved by whitening and PCA. However, the novelty of the method was fragmenting the hyperspectral cube into smaller cubes and running the ICA separately on the sub-cubes. The mixing vector that needs to be updated in each iteration of

ICA were partially updated for the processing of each sub-cube and then combined together to check for the convergence. The method was simply aimed to speed-up the convergence by executing sub-processes in a parallel manner.

Naanaa et al. [27] proposed a blind source separation technique assuming partially correlated source signals and constraining on the non-negativity of the source signals and mixing coefficients as in some real life problems. They developed some algebraic method of substitution for imposing the partial orthogonality of source signals and then solved the optimization problem using the constraint of non-negativity in a least-squares sense. The method was applied to NMR spectroscopy for determining the source organic compounds from the signal of a mixed compound. The method seemed to perform well even with varying amounts of noise. However, the algorithm was more time consuming than the FastICA, SOBI (Second-Order Blind Identification) or JADE algorithms.

Loghmari et al. [23] proposed a two-level source separation approach for separating the multispectral satellite images of a land cover into different sources and assigning a specific theme as humid, lake region, etc. for each source. The first level of source separation was blind source separation of the spectral bands without any prior knowledge of the sources. The authors considered the correlation between the observed multispectral images and the immediate neighbourhood of a pixel. The covariance matrices of the pixels with immediate neighbours and the correlation among the multispectral bands are jointly diagonalized using second-order statistics. Using Joint Diagonalization (JD) criterion allows the possibility of finding sources that are also Gaussian. The sources obtained using the spectral separation had reduced correlation with each other and hence were used for the spatial separation. The spatial separation based on Bayesian framework assigned a specific theme for each source by considering that a pixel was correlated with its 4-neighbourhood and thereby homogeneous regions specific to a theme could be obtained. The Bayesian framework assumed Gaussian priors for the sources, mixing matrix and the noise. When hypothesized priors are used, Maximum Likelihood (ML) approach is a better choice. But the assumed priors could be different from the original ones and therefore, the joint likelihood of the sources and the mixing matrix was combined with the assumed priors to form a Bayesian framework. The Baye's rule gave the joint *a posteriori* law to maximize and the criterion used for optimization was *Joint Maximum a Posteriori* (JMAP). The final sources obtained constituted extended homogeneous regions related to each theme and they had very low classification error compared to other methods of classification of land areas. This method of separation showed good results on homogeneous regions and average results on heterogeneous regions but mixed pixels were beyond the scope of the research.

The separation of multicomponent spectral datasets using Bayes estimation theory and Markov Chain Monte Carlo (MCMC) simulation methods was proposed by Moussaoui et al. [26]. The spectral mixture analysis aimed to extract the component spectra and the concentration

of the underlying species in the mixture. The statistical approach assumed complete independence of the component spectra and non-negativity of the pure component spectra and the concentration profiles. The Bayes framework defined the *a posteriori* density of the component spectra and the concentration profiles based on the priori knowledge of the mixture and the assumptions of the densities of the component spectra. Gamma distribution was chosen as *a priori* densities of the component spectra and the concentration profiles. The noise distribution model was chosen to be Gaussian. The estimation of the parameters of the Gamma and Gaussian distributions known as hyperparameters were made using the *Joint Maximum a Posteriori* (JMAP), *Marginal Maximum a Posteriori* (MMAP), Marginal Posterior Mean (MPM) estimates. Each prior model lead to a regularization criterion and these regularization parameters introduced in the posterior estimates ensured non-negativity of the pure spectra and the concentration profiles.

The primary objective of the MCMC technique was to simulate an ergodic markov chain that followed asymptotically the posterior density. Then the estimates of the component spectra and the mixing coefficients were made from the simulated markov chains. The results of the simulation showed a list of admissible solutions and the number of iterations required for convergence was empirical. Therefore, the computation time also increased for larger datasets. The assumption of Gamma distribution of the component spectra provided good results only when the amplitude of background signal was low. Therefore, some data pre-processing could have been necessary to reduce the effect of background signal.

A robust independent component analysis based on maximization of kurtosis was developed by Zarzoso et al. [45]. The algorithm showed the possibility of avoiding prewhitening and incorporating the knowledge of the kurtosis sign of the sources to be extracted to target specific sources, thus reducing the computational complexity and reduction of error accumulation. The method was applied for separating activities in Electro-Cardio-Graph (ECG) signals. The atrial activity signals in the atrial fibrillation and atrial flutter episodes typically lie in the sub-Gaussian space. While the fetal ECG from the maternal skins are normally impulsive and are super-Gaussian. Therefore, the alternative was to extract sources of known kurtosis.

Bingham et al. [5] extended the ICA method of kurtosis maximization using fixed-point algorithm to the extraction of complex-valued signals from convoluted mixtures. The algorithm proposed was robust against outliers and computationally simple.

Independent component analysis in biomedical image processing for extraction of the quantifications of melanin and haemoglobin was first attempted by Tsumura et al. [35]. A color RGB image of skin was processed to get three color channels separately. The three colour channels for each pixel was assumed to be the result of a linear combination of the pure components melanin and haemoglobin weighted by their quantities. Principal component analysis was applied to reduce the space of three color channels into the space of the two skin components. Independent

component analysis was then applied to estimate the separating matrix which was shown to be the inverse of the mixing matrix. The separating matrix was obtained by minimising the Burel's independence [7] value for the source pure component signals. The minimization was achieved using quasi-Newton optimization of the MATLAB toolbox. The independence values suggested that the source signals were quite independent of each other. The matrix for estimation of the quantities of each of the component or pigment was computed from the separating matrix. A color sysnthesis equation was used to display the quantifications of melanin and haemoglobin in two separate images.

Tsumura et al. [36] extended their work of separation and quantification of melanin and haemoglobin from skin images for the components' absorbance spectra and quantification from skin absorbance images. The skin colour images with three color channels was used as in their previous work. The spectral reflectance for each pixel was estimated using some lower-dimensional linear approximation from the R, G and B values of each pixel, thereby producing spectral reflectance images of skin over three wavelengths [19, 41]. The skin reflectance images were transformed into absorbance images using a logarithmic transformation. Independent component analysis as in their previous work was used to obtain the absorbance of melanin and haemoglobin and their respective quantifications in the skin absorbance images. The obtained spectral absorbances for melanin and haemoglobin were similar to that shown by Anderson et al. [1] by *in vitro* measurement.

Tsumura et al. [37,38] used an inverse optical scattering technique using multi-channel visible spectrum reflectance images to estimate the concentrations of skin melanin, oxy-haemoglobin and deoxy-haemoglobin. For the detection of specific diseases and diagnosing different skin colours, concentration of oxygen saturation in blood measured by oxy-haemoglobin is also important along with the other two components. The diffused spectral reflectance at each pixel of the skin image was calculated from the multi-channel image over the visible spectrum using Weiner estimation. The concentrations of the components were intially chosen randomly and the skin reflectance was simulated using Monte Carlo simulation based on the forward model of optical scattering in human skin. If the difference between the simulated skin reflectance and the measured skin reflectance was more than an error threshold then the concentration parameters were changed using a non-linear optimization method and the simulation was repeated until the simulated reflectance was close to the measured reflectance.

The mapping of pigmentation based on inverse optical scattering technique was expensive in time due to the Monte Carlo simulation based on forward optical scattering model and the inverse scattering technique performed by non-linear optimization. Therefore, Nakao et al. [28] developed a real-time system to map the pigmentation of skin from video sequences using pre-computed look-up tables for colour conversions. In the first table, RGB values from the video camera were converted in principal component scores. The RGB values were converted

to spectral reflectance using Weiner estimation and the spectral reflectance was then projected into the space of three principal components for three pigments. The second table, originally proposed in this work, converted the principal component scores into pigmentation values using inverse optical scattering. Since, the principal components effectively showed the variation of the reflectance spectra, this look-up table was considered very effective in estimating the pigmentation values. The third table was used to reproduce the pigmentation values into RGB values for display on the video monitor. The first and third tables were considered to be device dependent while, the second table was device independent.

Tsumura et al. [39] modified their work for extraction of haemoglobin and melanin components in [35], to synthesizing skin color and texture incorporating aging factor, alcohol consumption and tanning factor. They proposed a technique of removing shading in human skin and then performed the independent component analysis. The shading was removed using an inverse lighting technique based on the Lambert-Beer law. Also the color synthesis method used in their work previously was modified to produce more realistic colours.

The analysis of inflammatory and immunological skin diseases was done by Yamaguchi et al. [43] using a 16-band multispectral image and principal component analysis. Each pixel comprised of a 16-band vector of skin reflectance and the principal component analysis was performed on each pixel. The pixel vector was then reconstructed with the number of principal components that mostly represented the pixel i.e the normal part showing the spectral variations. This normal part was then subtracted from the multispectral pixel value producing a differential multispectral image. To enhance the image spectral feature related to a specific wavelength, the spectral value at the wavelength was multiplied by a weight factor and then the multispectral pixel value was added back to the differential multispectral images weighted at specific wavelengths. Applying this method, the spectral feature of an abnormal part was enhanced as a difference from the normal wavelength depending on a specific wavelength. Spectral colour enhancement algorithm was used to visualize the abnormalities related to skin components like melanin, haemoglobin and oxy-haemoglobin showing specific features at specific wavelengths.

Raman spectra provide complex and rich information about the chemical constituents of biological samples. Vrabie et al. [40] proposed to analyse paraffin-embedded skin biopsies of malignant and benign tumors in oncology researches by Raman spectroscopy and PCA and ICA methods. They showed that the commonly used principal component analysis (PCA) does not give physically interpretable estimators of the component spectra and their associated concentration profiles. Based on a linear model and taking into account the statistical properties of spectra, ICA provided a better estimate of the spectra of chemical constituents. The estimators of associated concentration profiles were not orthogonal and comprised of only positive values, in contrast to PCA. ICA allowed to model the paraffin by only three Raman spectra and

provided good estimators of underlying spectra of the human skin. In oncology, the retrieval of spectral features of different types of skin tumors is sufficient for their discrimination and therefore of great interest.

An algebraic method for source separation is non-negative matrix factorization proposed by Lee and Seung [22]. In this approach, least squares approximation is used to estimate the coefficients of the source components' spectra as well as the quantifications or mixing values of the sources in the mixed signal are constrained to be strictly positive. The method was applied by Sajda et al. [32] for recovering constituent spectra from data of 3D chemical shift imaging of the brain. This method however, did not assume that the source signals were independent which could be a fair consideration in certain cases.

# Chapter 3

## Methodology

### 3.1 Introduction

The ASCLEPIOS system is used to extract skin patches with known pathology. A spectral reflectance reconstruction algorithm developed by Mansouri et al. [24] based on artificial Neural networks is used to get the reconstructed spectral reflectance at each pixel. The spectral reflectance for each pixel is a 36-dimension vector sampled over a wavelength of visible spectrum range of  $430\text{ nm}$  to  $780\text{ nm}$  with a difference of  $10\text{ nm}$  wavelength.

This work proposes two algorithms for the separation of skin components reflectance spectra and their associated quantifications from the skin reflectance spectra for a spatial resolution of pixels. The first method is based on the independent component analysis of skin reflectance spectra similar to that used by Tsumura in [35]. However, the methodology for ICA estimation here, is different from that used by other authors. Absolute value of kurtosis maximisation is used as a measure of non-Gaussianity of the underlying source components, primarily assumed to be epidermal melanin and dermal haemoglobin. Since, the origin of the components lie in two different layers of the skin, the components' absorbance or reflectance spectra are assumed to be independent. The prior knowledge about the absorbance spectra [20,29] which by inverse logarithmic transformation gives the reflectance spectra of the underlying components, allowed the assumption of the non-Gaussianity of the source signals. The ICA estimation using fixed-point algorithm or FastICA provided good estimate of the melanin and the haemoglobin spectra with the quantifications of the same for each pixel producing two images.

The second method aims to separate the deoxy-haemoglobin and oxy-haemoglobin spectra from the skin reflectance spectra and estimate their associated quantifications for each pixel. The method assumes that the required components are dependent on each other and there-

fore uses a straight-forward matrix factorisation approach with least-squares estimation. The methods proposed in this work are described in details in the following sub-sections.

### 3.1.1 Independent Component Analysis with Principal Component Analysis

We have applied the FastICA for our problem of skin component separation to estimate the independent components as a measure of non-Gaussianity. In our work melanin and haemoglobin have been assumed as independent source components.

In ICA, an important criterion is, if there are  $m$  observed random variables,  $[v_1, v_2, \dots, v_m]^T$  forming  $\mathbf{V}$ , then, there are  $l$  source components  $[s_1, s_2, \dots, s_l]^T$  forming  $\mathbf{S}$  where,  $l \leq m$  [15]. The linear relationship between the mixture and the independent sources can be given by

$$\mathbf{V} = \mathbf{AS} \quad (3.1)$$

Here,  $\mathbf{A}$  is the  $m \times l$  mixing matrix of full-rank.

The choice of ICA for this problem is due to its ability to find non-Gaussian components. The problem of finding the mixing matrix  $\mathbf{A}$  and the non-Gaussian components  $s_i$ ,  $i = 1, 2, \dots, l$ , is solved by defining that  $s_i$  has unit variance and somehow reducing the task of estimating the full-rank matrix  $\mathbf{A}$  in to a square matrix.

In our experiment, it is required to estimate two independent components out of  $m$  mixtures (reflectance data of pixels). Therefore, it is required to find out the two best representations out of  $m$  representations. This is achieved by Principal Component Analysis (PCA). PCA not only reduces the dimensionality but also does a *spherering* or *prewhitening* of the data so that the task of finding the mixing matrix reduces to the task of estimating a square orthogonal matrix. The task of finding the independent components and the mixing matrix can now be divided into two parts. Firstly, the preprocessing of the observed data and then the optimization rule for components estimation.

#### Preprocessing by Whitening and Dimensionality Reduction

The observed data  $\mathbf{V}$  is linearly transformed using PCA such that

$$\mathbf{X} = \mathbf{MV} = \mathbf{MAS} = \mathbf{BS} \quad (3.2)$$

Where,  $\mathbf{B} = \mathbf{MA}$  is the orthogonal mixing matrix with the assumptions that the components have unit variance.

Therefore,

$$E \{ \mathbf{X} \mathbf{X}^T \} = \mathbf{B} E \{ \mathbf{S} \mathbf{S}^T \} \mathbf{B}^T = \mathbf{B} \mathbf{B}^T = \mathbf{I} \quad (3.3)$$

The problem is now reduced to the estimation of the orthogonal mixing matrix  $\mathbf{B}$ . The columns of the matrix  $\mathbf{B}$  are denoted by  $b_i$  and the  $i^{th}$  source component can be computed using  $\mathbf{X}$  by equation 3.4.

$$s_i = (b_i)^T \mathbf{X} = \mathbf{w}^T \mathbf{X} \quad (3.4)$$

Whitening of the observed data  $\mathbf{V}$  into  $\mathbf{X}$  by PCA reduces the dimensionality of  $\mathbf{V}$  from  $m$  to  $l$  and also ensures that the transformed data  $\mathbf{X}$  lie within a unit sphere, i.e. the covariance of  $\mathbf{X}$  is equal to identity. The mean of the observed data is removed to center the data about zero and then the covariance of the transpose of the observed data is computed. The significance of the transpose is that the required covariance matrix  $\mathbf{C}$  is of dimension  $m \times m$  that results in the sample size of the obtained source components' spectra to be the same as the sample size of the observed reflectance data of each mixed pixel. Eigen decomposition of the covariance matrix yields a diagonal matrix  $\mathbf{D}$  of eigen-values in ascending order and a matrix  $\mathbf{E}$  whose columns form the corresponding eigen-vectors associated with the eigen-values such that the relation in equation 3.5 holds.

$$\mathbf{C} = \mathbf{E} \mathbf{D} \mathbf{E}^T \quad (3.5)$$

The matrices  $\mathbf{E}$  and  $\mathbf{D}$  both are  $m \times m$ . To reduce the dimensions of  $\mathbf{E}$  to  $m \times l$  and  $\mathbf{D}$  to  $l \times l$  respectively, where,  $l$  is the number of source components to be extracted, the highest  $l$  eigen-values and their corresponding columns of  $\mathbf{E}$  are retained. The new whitened and reduced dimensioned data is represented in the reduced subspace of  $\tilde{\mathbf{E}}$  and  $\tilde{\mathbf{D}}$ .

$$\tilde{\mathbf{E}} = \begin{bmatrix} \mathbf{E}(1, m) & \mathbf{E}(1, m-1) \\ \mathbf{E}(2, m) & \mathbf{E}(2, m-1) \\ \vdots & \vdots \\ \mathbf{E}(m, m) & \mathbf{E}(m, m-1) \end{bmatrix}, \quad \tilde{\mathbf{D}} = \begin{bmatrix} \mathbf{D}(m, m) & 0 \\ 0 & \mathbf{D}(m-1, m-1) \end{bmatrix}$$

In our experiment,  $l = 2$  as there are two source components to be extracted. The whitening matrix  $\mathbf{M}$  can be represented as in equation 3.6.

$$\mathbf{M} = \tilde{\mathbf{D}}^{-1/2} \tilde{\mathbf{E}}^T \quad (3.6)$$

Therefore, the whitened data in the reduced subspace is

$$\mathbf{X} = \mathbf{M} \mathbf{V} = \tilde{\mathbf{D}}^{-1/2} \tilde{\mathbf{E}}^T \mathbf{V} \quad (3.7)$$

From equation 3.2 we have the following transformation.

$$\mathbf{A} = \mathbf{M}^{-1}\mathbf{B} \quad (3.8)$$

Where,  $\mathbf{M}^{-1}$  is the dewhitening matrix and is represented as

$$\mathbf{M}^{-1} = (\tilde{\mathbf{D}}^{-1/2}\tilde{\mathbf{E}}^T)^{-1} = \tilde{\mathbf{E}}\tilde{\mathbf{D}}^{1/2} \quad (3.9)$$

### Optimisation Using Fixed-Point Algorithm

The optimisation framework used in this work is based on the FastICA method developed by Hyvärinen et al. [16]. Kurtosis maximization as a measure of non-Gaussianity has been a classical technique to estimate the independent components. Due to the non-Gaussianity of the source components, kurtosis maximisation of the source components have been employed in this work. However, it is to be noted at this point that maximisation of kurtosis is basically maximising the absolute value of the kurtosis. This enables to extract both sub-Gaussian and super-Gaussian components with negative and positive kurtosis respectively. Kurtosis of a random variable  $y$  with zero mean can be defined as

$$kurt(y) = E\{y^4\} - 3(E\{y^2\})^2 \quad (3.10)$$

Aiming to maximise the non-Gaussianity i.e. the kurtosis of the independent components another constraint holds i.e.  $E\{y^2\} = 1$ . Which implies that, since the components are independent, they have unit variance. Therefore, using equation 3.4 the independent components can be estimated by maximisation of the kurtosis  $kurt(\mathbf{w}^T\mathbf{X})$  under the constraint  $E\{(\mathbf{w}^T\mathbf{X})^2\} = \|\mathbf{w}\|^2 = 1$ , that follows from equation 3.11 as  $\mathbf{X}$  is already whitened.

$$E\{y^2\} = E\{\mathbf{w}^2\} E\{\mathbf{X}^2\} = E\{\mathbf{w}^2\} = 1 \quad (3.11)$$

Therefore, in the optimization problem we seek for a vector  $\mathbf{w}$  such that the linear combination  $\mathbf{w}^T\mathbf{X}$  has the maximum non-Gaussianity.

The cost function for the optimization is defined as

$$J(\mathbf{w}) = E\{(\mathbf{w}^T\mathbf{X})^4\} - 3(E\{(\mathbf{w}^T\mathbf{X})^2\})^2 \quad (3.12)$$

The Lagrangian  $L(\mathbf{w}, \lambda)$  of the cost function in equation 3.12 using a penalty term for the constraint can be computed as follows using Kuhn-Tucker condition and Lagrange multiplier.

$$L(\mathbf{w}, \lambda) = E \{ (\mathbf{w}^T \mathbf{X})^4 \} - 3(E \{ (\mathbf{w}^T \mathbf{X})^2 \})^2 + \lambda(\|\mathbf{w}\|^2 - 1) \quad (3.13)$$

$$= E \{ (\mathbf{w}^T \mathbf{X})^4 \} - 3\|\mathbf{w}\|^4 + \lambda(\|\mathbf{w}\|^2 - 1) \quad (3.14)$$

Where,  $\lambda$  is the Lagrange multiplier.

Maximisation of the Lagrangian cost function would lead to a stable point where its gradient would be equal to zero. Therefore, the gradient of the Lagrangian function with respect to  $\mathbf{w}$  would be as follows.

$$\frac{\delta L(\mathbf{w}, \lambda)}{\delta \mathbf{w}} = 4 \left[ E \{ \mathbf{X}(\mathbf{w}^T \mathbf{X})^3 \} - 3\|\mathbf{w}\|^2 \mathbf{w} \right] + 2\lambda \mathbf{w} = 0 \quad (3.15)$$

The form of the penalty has been a function of  $\|\mathbf{w}\|^2$  only, therefore, irrespective of the form of the constraint, the gradient of the penalty term becomes a scalar multiplied with the vector  $\mathbf{w}$ . Therefore, solving algebraically, the fixed-point  $\mathbf{w}$  can be written as in equation 3.16, i.e. a stable point reaches where no change occurs to  $\mathbf{w}$  when the gradient is added to it.

$$\mathbf{w} = \text{scalar} \times \left[ E \{ \mathbf{X}(\mathbf{w}^T \mathbf{X})^3 \} - 3\|\mathbf{w}\|^2 \mathbf{w} \right] \quad (3.16)$$

The scalar value is insignificant and can be adjusted by normalization of the obtained value of  $\mathbf{w}$  by dividing it by its norm so that the constraint holds and it lies within a unit sphere. Using fixed-point iteration scheme, the update for the new value of the vector  $\mathbf{w}(t)$  can be written as a function of the old value  $\mathbf{w}(t-1)$ , where  $t$  is the iteration number (equation 3.17).

$$\mathbf{w}(t) = E \{ \mathbf{X}(\mathbf{w}(t-1)^T \mathbf{X})^3 \} - 3\mathbf{w}(t-1) \quad (3.17)$$

The iteration continues until the direction of the old and new values of  $\mathbf{w}$  are the same; i.e. the absolute value of the dot product of the two vectors is almost equal to one. After each update,  $\mathbf{w}$  is normalised to keep the vector within a unit sphere as in equation 3.18

$$\mathbf{w} = \mathbf{w} / \|\mathbf{w}\| \quad (3.18)$$

$\mathbf{w}$  , is a vector representing a column of the mixing matrix  $\mathbf{B}$  , therefore, only one source component is obtained using this method. The other components are obtained using the Gram Schmidt deflation approach [15] where a matrix  $\bar{\mathbf{B}}$  is formed with the already found  $\mathbf{w}$  vectors and the current estimate of  $\mathbf{w}(t)$  is projected back into the orthogonal space of  $\bar{\mathbf{B}}$  before the normalisation step (equation 3.19).

$$\mathbf{w}(t) = \mathbf{w}(t) - \bar{\mathbf{B}}\bar{\mathbf{B}}^T \mathbf{w}(t) \quad (3.19)$$

This step of decorrelation ensures that we do not obtain the same independent component. The dewhitened matrix  $\mathbf{A}$  is obtained using equation 3.8.

### 3.1.2 Non-Negative Matrix Factorization (NNMF)

Non-negative matrix factorization suggested by Lee and Seung [22] is a useful method of decomposition of multivariate data. The method explicitly enforces the nonnegativity constraint on the values of the source signals as well as the mixing quantities of the source signals forming the mixed data. The method does not constrain on the orthogonality of the source signals, hence, the source signals need not be the independent components of the multivariate mixed signal.

We reasonably assume that the source components that contribute to skin reflectance data and are dependent components might be oxy-haemoglobin ( $HbO_2$ ) and deoxy-haemoglobin ( $Hb$ ). Therefore, we have used this method of matrix factorization for the separation of multivariate skin reflectance data into its dependent source components and estimate the quantifications of each of these in the same.

The problem of source separation is formulated as a linear mixture separation problem as in equation 3.20.

$$\mathbf{X} = \mathbf{AS} + E \quad (3.20)$$

$\mathbf{X}$ , is the mixture of  $m$  rows and  $n$  columns with each row representing the spectral reflectance vector for each pixel.  $\mathbf{S}$ , is a matrix of  $l$  rows and  $n$  columns with  $l$  being the number of sources to be extracted. The matrix  $\mathbf{A}$  is known as the mixing matrix with  $m$  rows and  $l$  columns. The columns of which represent the mixing values of each source component. The noise matrix  $E$  can be reasonably assumed to be Gaussian noise that has resulted due to the sensors. However, to keep the formulation less complicated, we may ignore the noise in the estimation.

The nonnegativity constraint is enforced on the source signals and the mixing matrix as  $\mathbf{S} \geq 0$  and  $\mathbf{A} \geq 0$  respectively. Therefore, the problem can be formulated as a maximum-likelihood problem with least-squares solution as in equation 3.22.

$$\mathbf{A}_{ML}, \mathbf{S}_{ML} = \arg \max_{\mathbf{A}, \mathbf{S}} p(\mathbf{X} | \mathbf{A}, \mathbf{S}) \quad (3.21)$$

$$\Rightarrow F = \arg \min_{\mathbf{A}, \mathbf{S}} \|\mathbf{X} - \mathbf{AS}\|^2 \quad (3.22)$$

$$\text{Subject to : } \mathbf{A} \geq 0, \mathbf{S} \geq 0$$

In the maximum likelihood optimization, the negative log-likelihood of  $F$  is minimized i.e.  $\log \|\mathbf{X} - \mathbf{AS}\|$  is computed at each iteration. Here,  $\|\cdot\|$  is the Euclidean norm. The updates of  $\mathbf{A}$  and  $\mathbf{S}$  can be performed by using the gradient-descent algorithm. The derivatives of  $F$  with respect to  $\mathbf{A}$  and  $\mathbf{S}$  can be computed as in equation 3.23 and equation 3.24 respectively.

$$\frac{\partial F}{\partial \mathbf{A}} = -2 \times (\mathbf{XS}^T - \mathbf{ASS}^T) \quad (3.23)$$

$$\frac{\partial F}{\partial \mathbf{S}} = -2 \times (\mathbf{A}^T \mathbf{X} - \mathbf{A}^T \mathbf{AS}) \quad (3.24)$$

Therefore, the updates of  $\mathbf{A}$  and  $\mathbf{S}$  using the gradients are as shown in equation 3.25 and equation 3.26 respectively.

$$\mathbf{A} = \mathbf{A} + \delta(\mathbf{XS}^T - \mathbf{ASS}^T) \quad (3.25)$$

$$\mathbf{S} = \mathbf{S} + \gamma(\mathbf{A}^T \mathbf{X} - \mathbf{A}^T \mathbf{AS}) \quad (3.26)$$

The parameters  $\delta$  and  $\gamma$  can be considered as the learning rates of the additive update rule. Lee and Seung showed that by properly choosing these parameters, the additive update rule can be transformed into a multiplicative update rule that provides the same minimum as the former and also ensures that  $\mathbf{A}$  and  $\mathbf{S}$  are non-negative. Therefore, the parameters are modified as in equation 3.27 and equation 3.28.

$$\delta_{m \times l} = \frac{\mathbf{A}_{m \times l}}{(\mathbf{ASS}^T)_{m \times l}} \quad (3.27)$$

$$\gamma_{l \times n} = \frac{\mathbf{S}_{l \times n}}{(\mathbf{A}^T \mathbf{AS})_{l \times n}} \quad (3.28)$$

The multiplicative update rule takes the forms as in equation 3.29 and equation 3.30.

$$\mathbf{A}_{m \times l} = \mathbf{A}_{m \times l} \frac{(\mathbf{XS}^T)_{m \times l}}{(\mathbf{ASS}^T)_{m \times l}} \quad (3.29)$$

$$\mathbf{S}_{l \times n} = \mathbf{S}_{l \times n} \frac{(\mathbf{A}^T \mathbf{X})_{l \times n}}{(\mathbf{A}^T \mathbf{AS})_{l \times n}} \quad (3.30)$$

The notations used in the equation 3.27 - 3.30 are the same as the previous ones except that the subscripts indicate the final dimensions of the matrices to specify that the multiplication and division of matrices with same dimension are element-wise operations and not normal matrix multiplications.

The initialization of the matrix  $\mathbf{A}$  is done randomly with positive values and  $\mathbf{S}$  is initialized using least-squares estimation with a single constraint as given in equation 3.31.

$$\arg \min_{\mathbf{A}, \mathbf{S}} \|\mathbf{X} - \mathbf{AS}\|^2 \quad (3.31)$$

$$\text{Subject to : } \mathbf{S} \geq 0$$

The dimension  $n$  is 36 in our experiment since the reflectance data for each pixel is over 36 wavelengths sampled between 430 – 780 nm.

## Chapter 4

# Results and Discussions

The skin reflectance data obtained from the reconstructed seven set of mono-channel images called a multispectral image, for each pixel, is in terms of percentage values over 36 wavelengths sampled equally over  $430\text{ nm}$  to  $780\text{ nm}$ . Therefore, we have 36 set of reflectance planes of skin patches reconstructed from a multispectral image acquired by the device ASCLEPIOS within a visible range. Figure 4.4 shows the 36 reconstructed reflectance planes as images constituting the hyperspectral cube and figure 4.1 shows an example of the reflectance of a pixel. Each pixel is an observation in the form of a vector of 36 dimensions. The reflectance of the source components haemoglobin, oxy-haemoglobin and melanin can be computed by inverse logarithmic transformation of the absorbance as

$$\text{reflectance} = -\log_{10}(\text{absorbance}) \quad (4.1)$$

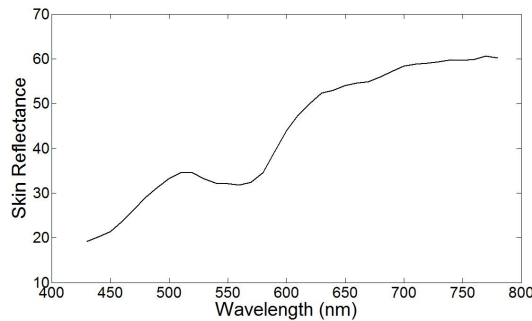


Figure 4.1: Reconstructed reflectance of a pixel.

Figure 4.2 shows the reflectance spectra of the skin source components computed using the

data from Jacques [20] and Prahl [29].

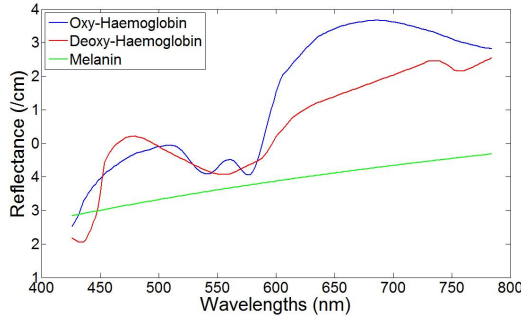


Figure 4.2: Ideal Reflectance Spectra for Oxy-haemoglobin, Deoxy-haemoglobin and Melanin

## Mixing Matrix to Quantification Images

The mixing matrix obtained from the methods comprise of two columns, each column corresponding to the mixing quantities in each pixel for one source. Each column is then rearranged into a 2D matrix using the dimension of the rows and columns of the skin patch used in the experiment. For the ICA estimation since the values of the mixing matrix can be both positive and negative values, these are normalised within the gray level range [0 – 255] with the minimum value and maximum value of each column. This results in two gray level images corresponding to the quantifications of each of the sources. The prior knowledge about the nature of the reflectance spectrum of each of the sources enables manual identification of the column of the mixing matrix corresponding to the first source component or second component.

## Fitting of Melanin Data and Re-estimation of the Mixing Matrix

The source spectrum obtained for melanin in the ICA method is noisy but, very closely resemble the ideal reflectance. There have been a few researches previously that tried to fix the obtained melanin spectrum [21, 42]. Therefore, we proposed a method of fixing the melanin spectrum using a polynomial fit and re-estimate the mixing vector associated with this source component.

The polynomial fit used is a straight line regression fit in least-squares sense. If there are  $n$  points as  $(x_1, y_1), (x_2, y_2), \dots, (x_n, y_n)$  and have to be fitted with a straight line  $Y = mX + b$ , then the slope  $m$  and the intercept  $b$  of the line may be estimated using the equation 4.2 and 4.3.

$$m = \frac{n \sum_i x_i y_i - \sum_i x_i \sum_i y_i}{n \sum_i x_i^2 - (\sum_i x_i)^2} \quad (4.2)$$

$$b = \frac{1}{n} (\sum_i y_i - m \sum_i x_i) \quad (4.3)$$

Figure 4.3 shows the obtained melanin and haemoglobin spectra before and after polynomial fit of melanin.

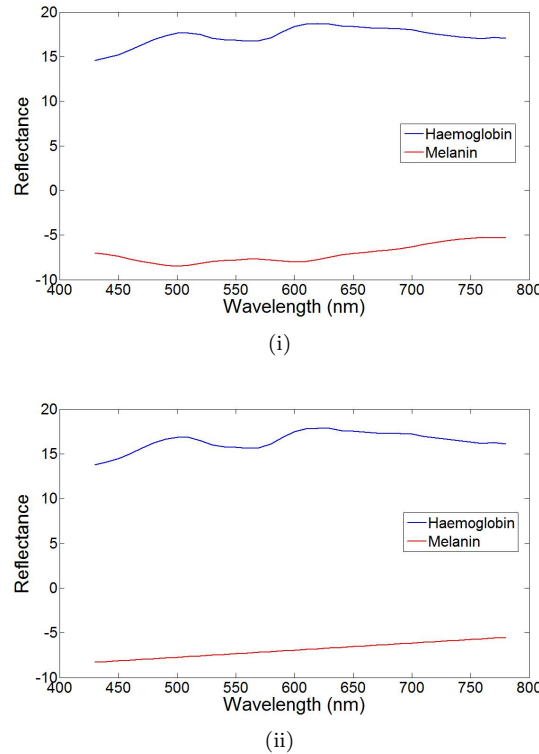


Figure 4.3: (i) Melanin and haemoglobin spectra obtained before fitting, (ii) Haemoglobin and melanin spectra after polynomial fit.

Since the obtained components with their mixing quantities hold a linear relationship to form the observed mixture. We compute the mixture by the following:

`mixture = melanin×mixing_vector_melanin + haemoglobin×mixing_vector_haemoglobin`

Then we subtract the proportion of haemoglobin from this mixture and call it  $X_m$ . The

fitted melanin spectrum is called  $Mel_{fix}$  and therefore, the new quantification of the melanin is obtained using the equation 4.4.

$$vec_{mel} = X_m / Mel_{fix} \quad (4.4)$$

Since,  $X_m$  is a matrix that is not square and  $Mel_{fix}$  is a vector, the solution to such kind of right '/' division in MATLAB is the solution to  $vec_{mel}$ , where,  $vec_{mel} \cdot Mel_{fix} = X_m$  in least-squares sense for under or over-determined systems.

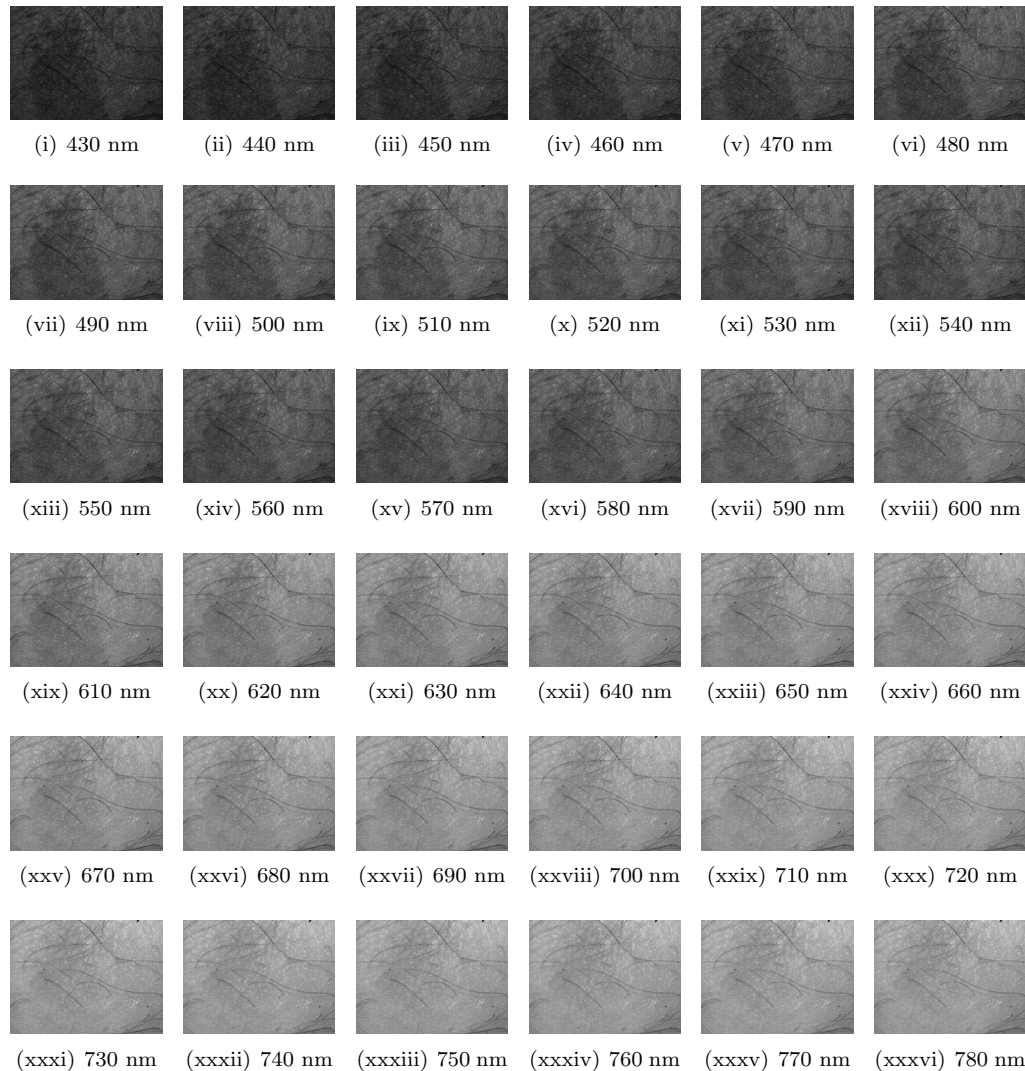


Figure 4.4: Reconstructed reflectance images.

## 4.1 Results for FastICA

This method of FastICA was applied on the skin reflectance data of a specific pathology known as 'café-au-lait' meaning 'coffee with milk'. These are hyperpigmented lesions found in skin or iris due to increased content of melanin. This method considers the two independent component spectra as haemoglobin and melanin and extracts the same along with the mixing matrix whose columns are normalised and represent quantifications of each independent component. It is to be noted that, since, the absolute value of kurtosis is maximised, the sources obtained might be the inverse of what is desired, therefore, the sources are reversed if required with user input dynamically. The quantifications are converted into gray scale images shown in figure 4.5. The advantage of this Fast ICA method is that the convergence is often in 5 – 6 steps; therefore, it is computationally less expensive than the gradient-descent algorithms. Also, it was shown by Hyvärinen [16] that the algorithm always converges and the convergence is cubic. However, a significant amount of computation might be needed to compute the covariance matrix if the size of skin patch is too large.

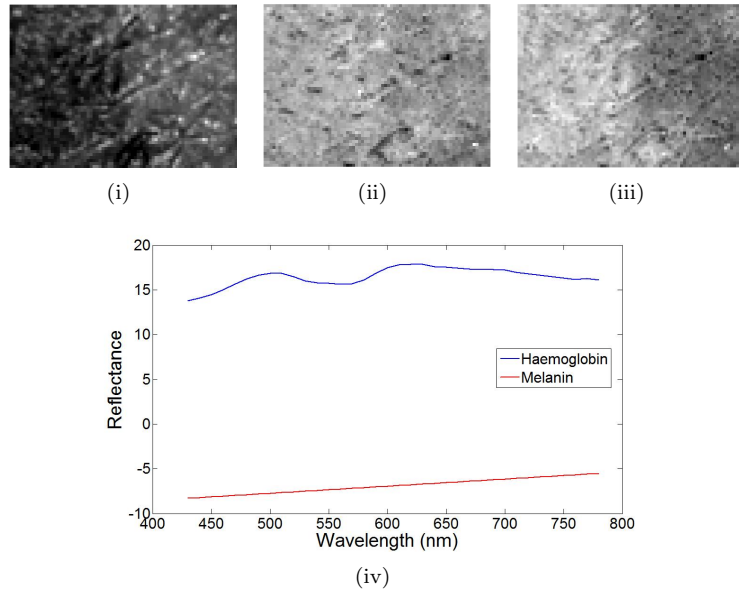


Figure 4.5: Independent component analysis (i) Original skin patch, (ii) Supposed to be haemoglobin quantification, (iii) Supposed to be melanin quantification, (iv) haemoglobin and melanin spectra.

The sample patch that was processed contained portions of lightly pigmented 'café au lait' spot and normal skin on the left and right parts of the original image respectively figure 4.5(i). Therefore, in figure 4.5(iii) it is evident that the melanin is more quantified on the left part of

the image with black spots embedded that characterise the milky spots in the region having less melanin. Figure 4.5(ii) shows an almost uniform quantification of haemoglobin over the same patch. The spectrum obtained for haemoglobin and corrected melanin closely resemble the ideal spectra.

Additionally, almost homogeneous patches from only normal part and only 'café au lait' spot were processed separately and histogram analysis was done with the obtained quantification images along with that of the patch used in figure 4.5.

The histograms in figure 4.6(vi) and figure 4.6(iv) show single mode peaks that suggest that both have almost uniform quantifications. The peak in figure 4.6(vi) is almost center skewed, while that in figure 4.6(iv) is right skewed. This suggests that the patch has more quantification of melanin and less of haemoglobin as the patch was taken only from the café-au-lait part of the skin.

The patch in figure 4.7(i) was taken from the normal part of the skin. Figure 4.7(vi) shows a little right skewed peak than figure 4.7(iv) which suggests that the haemoglobin quantification in normal parts of skin is more than the melanin quantification for Caucasian skins.

The patch used figure 4.8(i) is the same used in figure 4.5(i) and consists of a junction of café-au-lait spot and normal part. The histogram in figure 4.8(iv) shows two-modes or peaks that suggests less and more quantifications of melanin in the normal and café-au-lait parts respectively. While, the histogram in figure 4.8(vi) shows an almost center skewed single peak that suggests a uniform quantification of the haemoglobin over the patch.

## 4.2 Results of NNMF

The same café-au-lait patch was used for processing. Since, this process aims to separate oxy-haemoglobin and deoxy-haemoglobin, the choice of such a pathology is not very relevant. Instead a diseased skin patch with significant differences in deoxy- and oxy-haemoglobin content or an image of a slapped part of skin would be more relevant. However, the source spectra obtained very closely resemble the ideal oxy-haemoglobin and deoxy-haemoglobin spectra and quantifications are also obtained. But, no conclusion about the feasibility of the quantifications of the components can be drawn at this stage of the research.

The method based on non-negative matrix factorization was applied to the observed data and the iteration converged at the point where the current log-likelihood is greater than the previous log-likelihood. The number of iterations required to converge is more than 1000. Sometimes the log-likelihood does not tend to converge; in that case the iteration is stopped at a maximum of 10000 iterations. This method has less mathematical complexity, but, the computation for the optimization is expensive in time than the other method.

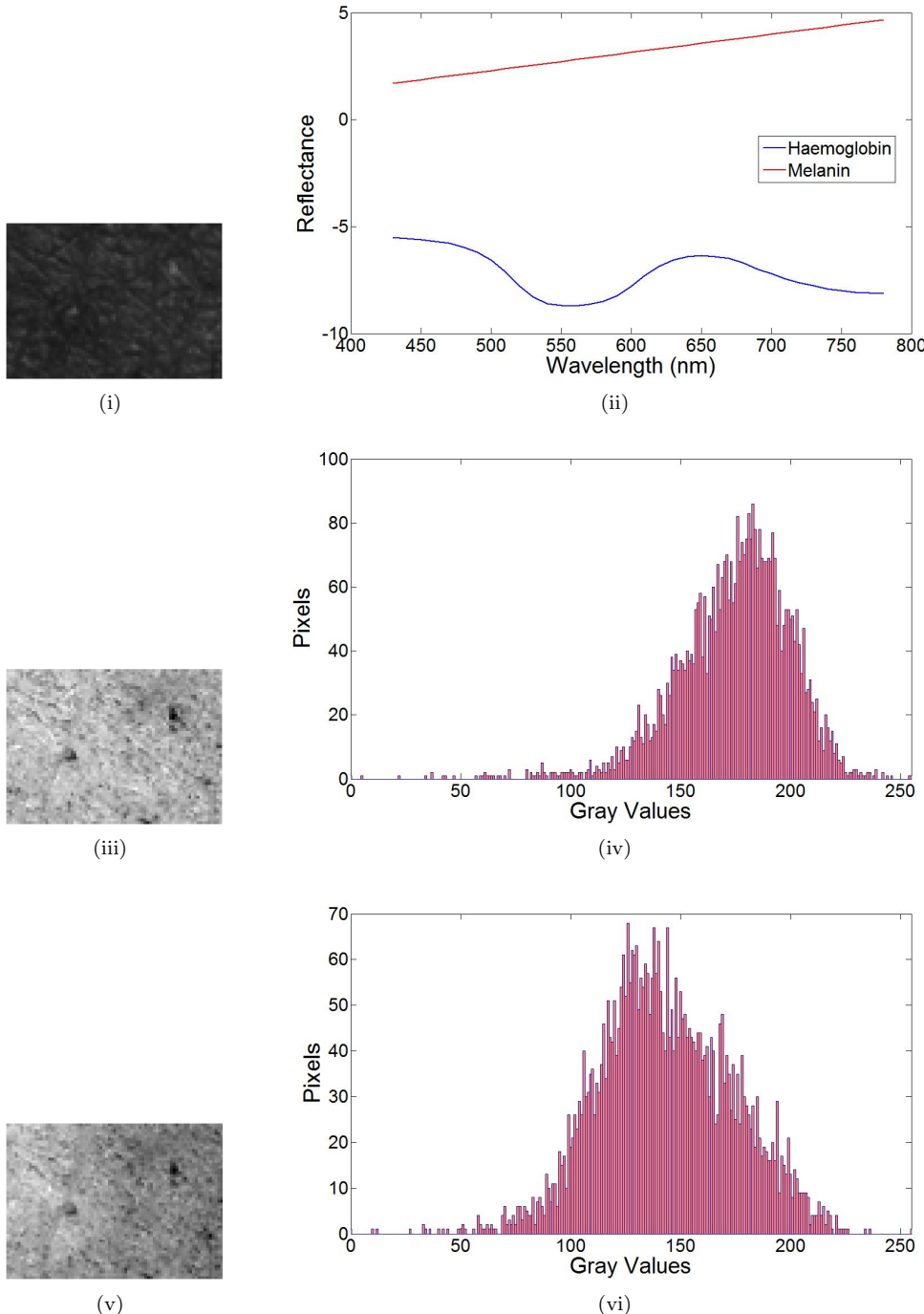


Figure 4.6: (i) Skin patch from café-au-lait spot, (ii) Obtained source spectra, (iii) Melanin quantification, (iv) Histogram of melanin quantification, (v) Haemoglobin quantification, (vi) Histogram of haemoglobin quantification

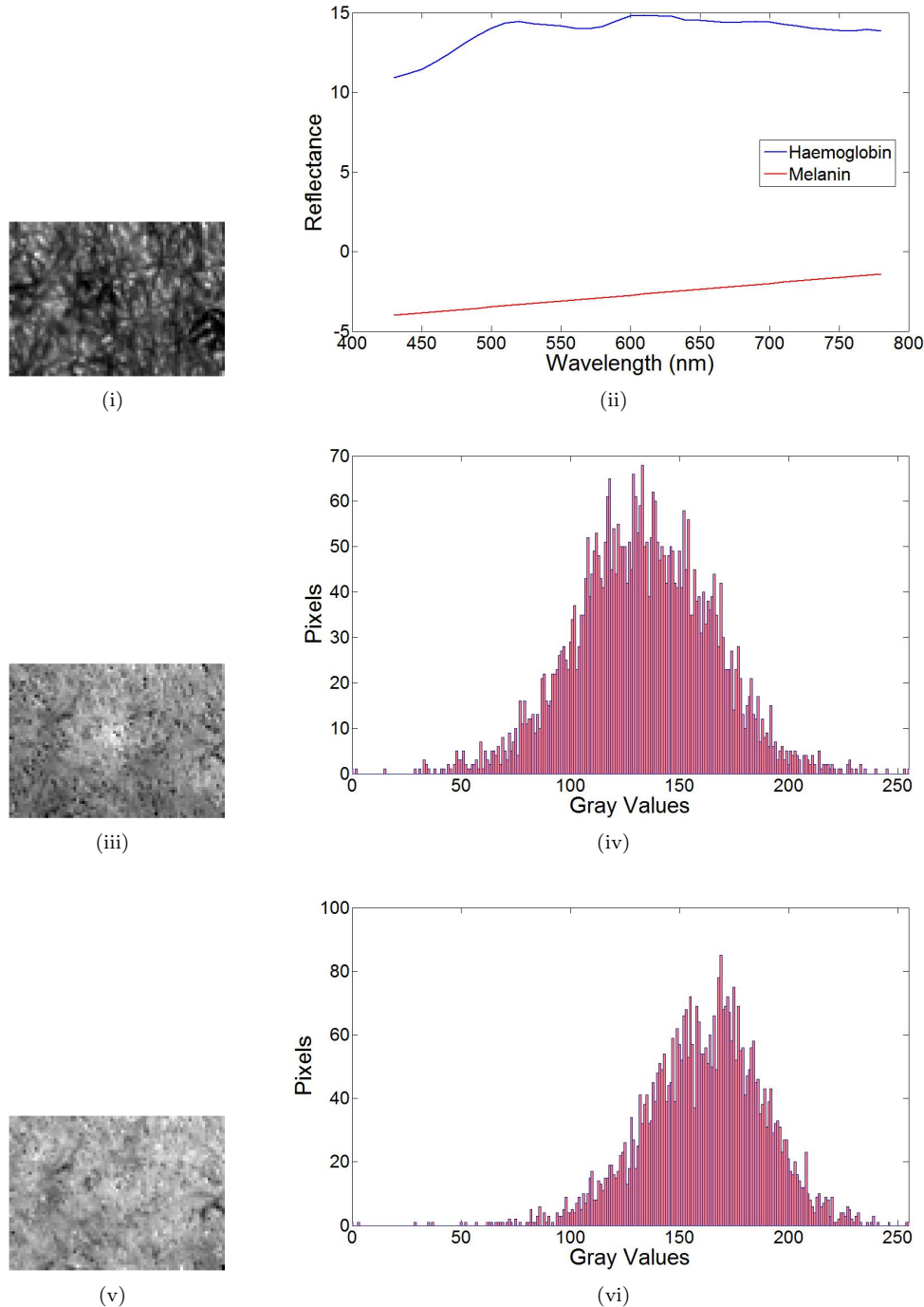


Figure 4.7: (i) Skin patch from normal part, (ii) Obtained source spectra, (iii) Melanin quantification, (iv) Histogram of melanin quantification, (v) Haemoglobin quantification, (vi) Histogram of haemoglobin quantification

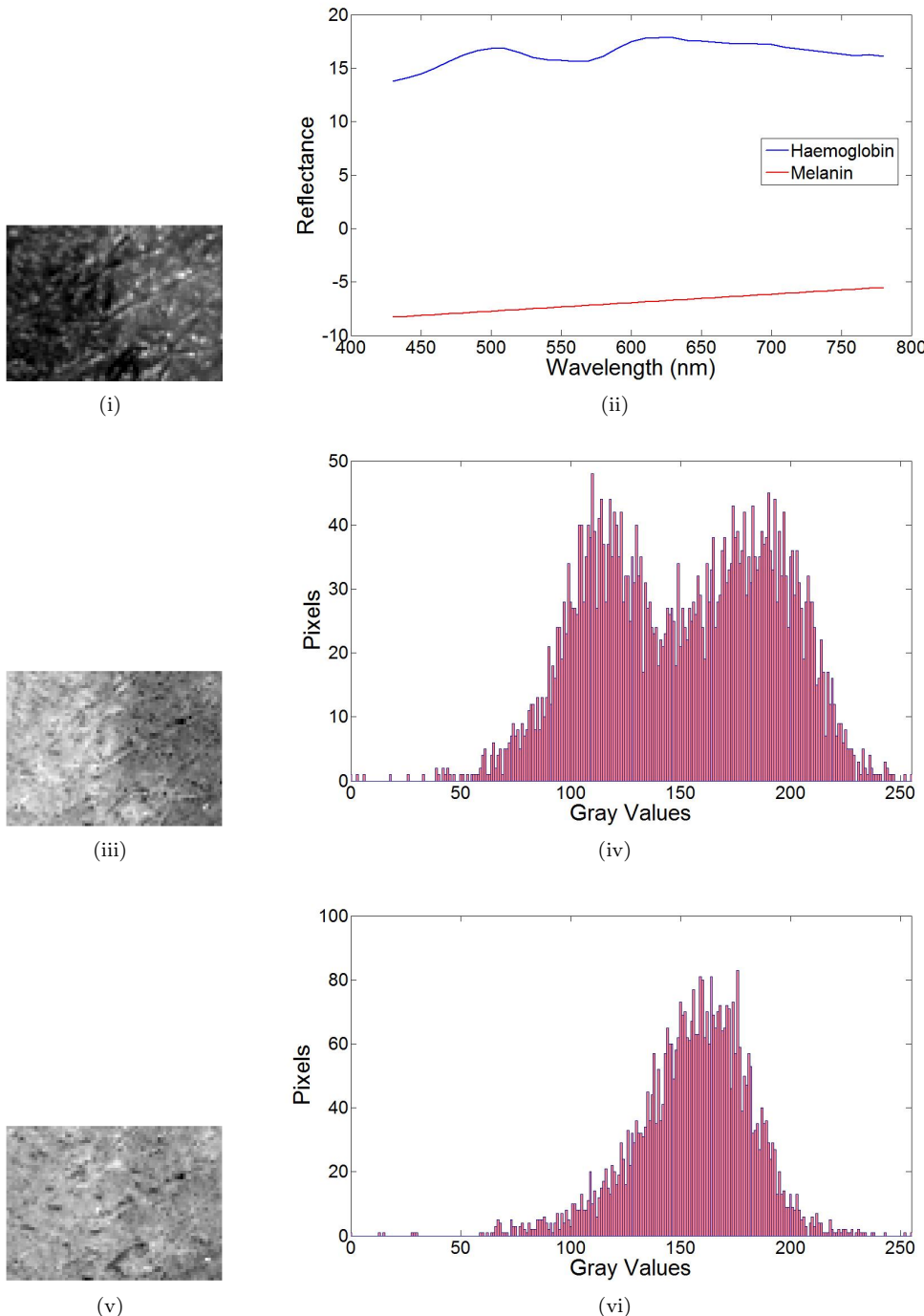


Figure 4.8: (i) Skin patch comprising both café-au-lait and normal parts, (ii) Obtained source spectra, (iii) Melanin quantification, (iv) Histogram of melanin quantification, (v) Haemoglobin quantification, (vi) Histogram of haemoglobin quantification

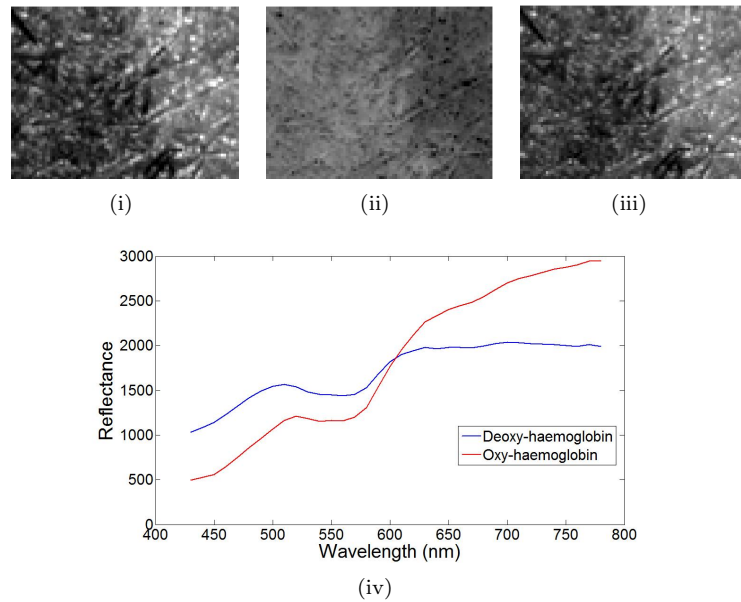


Figure 4.9: Non-negative Matrix Factorization (i) Original skin patch, (ii) Supposed to be oxy-haemoglobin quantification, (iii) Supposed to be deoxy-haemoglobin quantification, (iv) oxy- and deoxy-haemoglobin spectra.

Figure 4.9 shows the patch used, with the possible quantification images of oxy-haemoglobin and deoxy-haemoglobin and the obtained source spectra.

## Chapter 5

# Conclusions and Future Works

Techniques to separate various components underlying the skin and that are responsible for the effective skin reflectance spectra have been proposed and implemented in this thesis. An effective technique that is based on independent component analysis and principal component analysis have been implememnted to separate the possible independent components like melanin and haemoglobin and estimate the quantifications associated with each of these components. The results obtained using this technique show feasible quantifications of melanin and haemoglobin when tested on a 'café-au-lait' patch that causes pigmentation only due to the excess of melanin. Histogram analysis of different regions of such a patch compared to the normal part of the skin further prove the applicability of the method. The algorithm itself is not computationally expensive, however, the computation of covariance matrix for all pixels require a significant computation time. The current implementation has been done in MATLAB and therefore to avoid 'out-of-memory' problems smaller patches are used as input to the algorithm. However, it is expected that the computation of the covariance matrix would be faster in C/C++ and will not result in memory problems. The test has been performed using the 'café-au-lait' spot of only one patient where the result is consistent on every execution. However, it is assumed that the algorithm will provide consistent and feasible results for all such melanin pigmentations. This method can also be used for quantification of haemoglobin that is very important in diagnosing erythema that is a 'reddish' inflammation of skin due to the dilation of blood vessels in the skin dermis.

ICA estimation is sensitive to noisy data. Therefore, the method can be extended in future for pixel-wise extraction of melanin and haemoglobin based on the reduction of reflectance spectrum of each pixel which might provide better pixel-wise quantifications. Also other nonlinearities as contrast function may be used to provide accurate estimation of the components and their correponding quantifications. Though the components oxy- and deoxy-haemoglobin

are assumed to be dependent components, ICA method applied on the residual mixture after subtraction of the extracted melanin portion could yield components that could be assumed to be oxy- and deoxy-haemoglobin respectively. For further validation this method could be tested on a skin pathology called 'vitiligo' that is whitening of the skin due to absence of melanin.

The results obtained from the non-negative matrix factorization algorithm show relevant oxy-haemoglobin and deoxy-haemoglobin source spectra. However, the feasibility of quantifications of the same components have not been determined due to the unavailability of proper pathologies to be diagnosed. The method is simple in its mathematical logic, but the optimization takes more number of iterations to converge than the ICA method. Also, there is no guarantee of convergence always, therefore, the iterations are stopped after an allowed maximum number of iterations.

In this work, we have primarily focussed on the method of ICA for separating skin components. Therfore we may conclude that the system ASCLEPIOS along with this technique of source separation can make significant contribution to the research of non-invasive techniques for the diagnosis of skin diseases.

# Bibliography

- [1] R.R. Anderson and J.A. Parrish. The optics of human skin. *Journal of Investigative Dermatology*, 77:13–19, 1981.
- [2] E. Angelopoulou, R. Molana, and K. Daniilidis. Multispectral skin color modeling. Technical Report MS-CIS-01-22, June 2001.
- [3] A. N. Bashkatov, E. A. Genina, V. I. Kochubey, and V. V. Tuchin. Optical properties of human skin, subcutaneous and mucous tissues in the wavelength range from 400 to 2000nm. *Journal of Physics D: Applied Physics*, 38:2543–2555, 2005.
- [4] Adel Belouchrani, Karim Abed-Meraim, and J.-F. Cardoso. A blind source separation technique using second-order statistics. *IEEE Trans. on Signal Processing*, 45(2):434–444, 1997.
- [5] E. Bingham and A. Hyvärinen. A fast fixed-point algorithm for independent component analysis of complex valued signals. *Intl. Journal of Neural Systems*, 10(1):1–8, 2000.
- [6] C.F. Bohren and D. Huffman. *Absorption and scattering of light by small particles*. John Wiley, New York, 1983.
- [7] G. Burel. Blind separation of sources: a nonlinear neural algorithm. *Neural Networks*, 5:937–947, 1992.
- [8] J.-F. Cardoso. Source separation using higher order moments. *Proc. IEEE Int. Conf. on Acoustics, Speech and Signal Processing (ICASSP'89)*, pages 2109–2112, 1989.
- [9] J.-F. Cardoso. Eigen-structure of the fourth-order cumulant tensor with application to the blind source separation problem. In *Proc. IEEE Int. Conf on Acoustics, Speech and Signal Processing (ICASSP'90)*, pages 2655–2658, 1990.
- [10] J.-F. Cardoso and A. Souloumiac. Blind beamforming for non gaussian signals. *IEE Proceedings-F*, 140(6):362–370, 1993.

- [11] P. Comon. Independent component analysis-a new concept? *Signal Processing*, 36:287–314, 1994.
- [12] J. B. Dawson, D. J. Barker, D. J. Ellis, E. Grassam, J. A. Cotterill, G. W. Fisher, and J. W. Feather. A theoretical and experimental study of light absorption and scattering by *in vivo* skin. *Physics in Medicine and Biology*, 25(4):695–709, 1980.
- [13] I. R. Farah, M. B. Ahmed, and M. R. Boussema. Multispectral satellite image analysis based on the method of blind separation and fusion of sources. *Proc. of IEEE Intl. Geoscience and Remote Sensing Symposium*, 6:3638–3640, 2003.
- [14] A. Hyvärinen. Fast and robust fixed-point algorithms for independent component analysis. *IEEE Trans. on Neural Networks*, 10(3), 1999.
- [15] A. Hyvärinen, J. Karhunen, and E. Oja. *Independent Component Analysis*. John Wiley, New York, 2001.
- [16] A. Hyvärinen and E. Oja. A fast fixed-point algorithm for independent component analysis. *Neural Computation*, 9:1483–1492, 1997.
- [17] Aapo Hyvärinen and Erkki Oja. Independent component analysis:algorithms and applications. *Neural Networks*, 13(4-5):411–430, 2000.
- [18] Takanori Igarashi, Ko Nishino, and Shree K. Nayar. The appearance of human skin. Technical Report CUCS-024-05, Dept. of Computer Sc.,Columbia University, New York, USA, June 2005.
- [19] F. H. Imai, N. Tsumura, H. Haneishi, and Y. Miyake. Principal component analysis of skin color and its application to colorimetric color reproduction on crt display and hardcopy. *Journal of Image Science and Technology*, 40(5):422–430, 1996.
- [20] S. L. Jacques. Optical absorption of melanin. *Oregon Medical Laser Center Monthly news and articles on Biomedical Optics and Medical Lasers*, <http://omlc.ogi.edu/spectra/melanin/index.html>, 1998.
- [21] N. Kollias and A. H. Baqer. Absorption mechanisms of human melanin in the visible, 420-720 nm. *Journal of Investigative Dermatology*, 89(4):384–388, 1987.
- [22] D.D. Lee and H.S. Seung. Learning the parts of objects by non-negative matrix factorization. *Nature*, 401:788–791, 1999.

- [23] M. A. Loghmari, M. S. Naceur, and M. R. Boussema. A spectral and spatial source separation of multispectral images. *IEEE Trans. on Geoscience and Remote Sensing*, 44(12):3659, 2006.
- [24] A. Mansouri, F. S. Marzani, and P. Gouton. Neural networks in two cascade algorithms for spectral reflectance reconstruction. *ICIP*, 2:718–721, 2005.
- [25] J. A. McGrath, R. A. Eady, and F. M. Pope. *Rook's Textbook of Dermatology (Seventh Edition)*. Blackwell Publishing, 2004.
- [26] S. Moussaoui, C. Carteret, D. Brie, and A. Mohammad-Djafari. Bayesian analysis of spectral mixture data using markov chain monte carlo methods. *Chemometrics and Intelligent Laboratory Systems*, 81:137–148, 2006.
- [27] W. Naanaa and J.-M. Nuzillard. Blind source separation of positive and partially correlated data. *Signal Processing*, 85:1711–1722, 2005.
- [28] D. Nakao, N. Tsumura, and Y. Miyake. Real-time multi-spectral image processing for mapping pigmentation in human skin. *IS&T/SID's 9th Color Imaging Conference, Color Science, Systems and Appl.*, pages 80–84, 2001.
- [29] S. Prahl. Optical absorption of hemoglobin. *Oregon Medical Laser Center Monthly news and articles on Biomedical Optics and Medical Lasers*, <http://omlc.ogi.edu/spectra/hemoglobin/index.html>, 1999.
- [30] G. Prota, M. D'Ischia, and A. Napolitano. *The chemistry of melanins and related metabolites*, in 'The Pigmentary System'. Oxford University Press, 1988.
- [31] S. A. Robila. Distributed source separation algorithms for hyperspectral image processing. *Proceedings of the SPIE*, 5425:628–635, 2005.
- [32] P. Sajda, S. Du, T. Brown, L. Parra, and R. Stoyanova. Recovery of constituent spectra in 3d chemical shift imaging using non-negative matrix factorization. *Proc. International Conference on Independent Component Analysis and Blind Signal Separation (ICA'2003)*, pages 71–76, 2003.
- [33] M. Shimada, Y. Yamada, M. Itoh, and T. Yatagai. Melanin and blood concentration in human skin studied by multiple regression analysis: experiments. *Physics in medicine and Biology*, 46:2385–2395, 2001.
- [34] G. N. Stamatas, B. Z. Zmudzka, N. Kollias, and J. Z. Beer. In vivo measurement of skin erythema and pigmentation: new means of implementation of diffuse reflectance spectroscopy with a commercial instrument. *British Journal of Dermatology*, 159:683–690, 2008.

- [35] N. Tsumura, H. Haneishi, and Y. Miyake. Independent component analysis of skin color image. *J. Opt. Soc. Am. A*, 16(9):2167–2176, 1999.
- [36] N. Tsumura, H. Haneishi, and Y. Miyake. Independent component analysis of spectral absorbance image in human skin. *Optical Review*, 7(6):479–482, 2000.
- [37] N. Tsumura, M. Kawabuchi, H. Haneishi, and Y. Miyake. Mapping pigmentation in human skin by multivisible-spectral imaging by inverse optical scattering technique. *Proc. 8th Color Imaging Conference*, pages 81–84, 2000.
- [38] N. Tsumura, Y. Miyake, and F. H. Imai. Medical vision: measurement of skin absolute spectral reflectance image and the application to component analysis. *Proceedings of the 3rd International Conference on Multispectral Color Science (MCS'01)*, pages 25–28, 2001.
- [39] N. Tsumura, N. Ojima, K. Sato, M. Shiraishi, H. Shimizu, H. Nabeshima, S. Akazaki, K. Hori, and Y. Miyake. Image-based skin color and texture analysis/synthesis by extracting hemoglobin and melanin information in the skin. *Proceedings of ACM SIGGRAPH*, 22(3):770–779, 2003.
- [40] V. Vrabie, C. Gobinet, O. Piot, A. Tfayli, P. Bernard, R. Huez, and M. Manfait. Independent component analysis of raman spectra: Application on paraffin-embedded skin biopsies. *Biomedical Signal Processing and Control*, 2:40–50, 2007.
- [41] M. J. Vrhel and H. J. Trussell. Color correction using principal components. *Color Research and Application*, 17(5):328–338, 1992.
- [42] S. Xu, X. Ye, Y. Wu, F. Giron, J. L. Leveque, and B. Querleux. Automatic skin decomposition based on single image. *Computer Vision and Image Understanding*, 110:1–6, 2008.
- [43] M. Yamaguchi, M. Mitsui, Y. Murakami, H. Fukuda, N. Ohyama, and Y. Kubota. Multispectral color imaging for dermatology: application in inflammatory and immunologic diseases. *IS&T/SID 13th Color Imaging Conference*, 2005.
- [44] Tadamasa Yamamoto, Hirotugu Takiwaki, Seiji Arase, and Hiroshi Ohshima. Derivation and clinical application of special imaging by means of digital cameras and image j freeware for quantification of erythema and pigmentation. *Skin Research and Technology*, 14:26–34, 2008.
- [45] V. Zarzoso and P. Comon. Robust independent component analysis for blind source separation and extraction with application in electrocardiography. *30th Annual International Conference of the IEEE Engineering in Medicine and Biology Society*, 2008.